Supporting information for:

1,2,3-Triazolyl functionalized thiophene, carbazole and fluorene based A-*alt*-B type π-conjugated copolymers for sensitive and selective detection of aqueous and vapor phase nitroaromatics (NACs)

Dipanjan Giri[a] and Sanjib K. Patra[*a]

Department of Chemistry, IIT Kharagpur, Kharagpur 721302, WB, INDIA

1.		Materials and methods	S2-S3
2.		Synthesis and characterization	S3-S23
	2a.	Syntheses	S3-S6
	2b.	NMR spectra	S7-S19
	2c.	Mass spectrometry	S20-S21
	2d.	FTIR spectrum (measured as KBr pellets)	S21-S22
	2e.	Thermal studies (TGA) for the polymers	S23
3.		Photophysical and sensing studies	S23-S35
	3a.	Determination of quantum yield	S23
	3b.	Determination of lifetime	S23-S24
	3c.	Concentration dependent PL study and particle size determination by DLS	S24-S25
	3d.	Titration studies towards nitroaromatics	S25-S28
	3e.	Stern-Volmer plot	S29-S30
	3f.	Limit of detection	S30-S31
	3g.	Preparation of thin film of the polymer probes for the sensing studies	S31-S32
	3h.	Detection of aqueous PA sample by polymer thin film probes	S32-S33
	3i.	Repeatability study	S33-S34
	3j.	Contact mode detection	S34-S35
4.		^{1}H NMR titration of the probe with PA	S36-S37
5.		Electrochemical characterization	S37
6.		FESEM analysis	S38-S40
7.		Computational studies	S40-S43
8.		References	S43-S44

1. Materials and methods

All the air and moisture sensitive reactions and manipulations were carried out under an atmosphere of pre-purified Ar or N_2 by using dual manifold standard Schlenk techniques. Tetrahydrofuran and toluene were dried over Na/benzophenone. Dry DCM, $CHCl_3$ and 1,2-DCE were obtained by distillation over CaH_2 whereas MeOH and EtOH were dried by Mg cake and stored on 3 Å molecular sieves. Solvents used for all the cross-coupling and polymerizaton reactions were degassed (three times) *via* freeze-pump-thaw technique. Unless otherwise mentioned all the chemicals were of analytical grade, obtained from Aldrich, and used without further purification. Silica gel (60-120 mesh) and alumina, used for column chromatography were purchased from SRL, India. Eluting systems for column chromatography purifications were determined by thin layer chromatography (TLC) analysis. TLC plates were visualized under UV light (254 nm) or in iodine chamber.

^1H (600MHz, 400 MHz), $^{13}C\{^1H\}$ (125 MHz, 100 MHz) NMR spectra were obtained from Bruker Lambda spectrometer using $CDCl_3$ unless otherwise mentioned. Spectra were internally referenced to residual solvent peaks (δ = 7.26 ppm for proton and δ = 77.2 ppm for carbon (middle peak) for $CDCl_3$). All coupling constants (*J*) are given in Hz. The absorption and fluorescence spectra were collected using a Shimadzu spectrophotometer (Model UV-2450) and a Shimadzu spectrofluorimeter (Model RF-6000), respectively. FTIR spectroscopy was recorded in Spectrum-BX (Perkin Elmer). Solid state PL spectra were recorded using Flurolog Horiba (Model FL-1016, Spectracq). Molecular weights and polydispersity indices (PDI = M_w/M_n) of the polymers were obtained by Malvern tetradetector Gel Permeation Chromatography (GPC) using a Viscotek VE 2001 equipped with automatic sampler, pump, injector, inline degasser, column oven (30 °C), styrene/divinylbenzene columns with pore sizes of 500 Å and 100,000 Å, VE 3580 refractometer, four-capillary differential viscometer and 90° angle laser, low angle laser (7°) light scattering detector (VE 3210 & VE270) including UV-vis detector. HPLC grade THF was used as the chromatography eluent, at a flow rate of 1.0 mL/min. Samples were dissolved in the eluent (1 mg/mL) and filtered with a PTFE syringe filter (polytetrafluoroethylene membrane of 0.20 μm pore size) before analysis. Calibration of all four detectors (refractive index, laser light scattering, UV-vis and viscometry) was performed using polystyrene standards (Viscotek). This equipment allows the absolute measurement of homopolymer molecular weights and PDIs. Cyclic voltammetric studies were performed on a BASi Epsilon electrochemical workstation. CV of thin film polymer sample was measured by drop casting of the polymer solution on GC electrode, which was used as a

working electrode. The electrochemical study was conducted in CH_3CN with 0.1 M tetra-n-butylammonium hexafluorophosphate ($TBAPF_6$) as the supporting electrolyte. The reference electrode was Ag/AgCl and the auxiliary electrode was a Pt wire. The ferrocene/ferrocenium couple occurs at $E_{1/2}$ = +0.51 (70) V versus Ag/AgCl under the same experimental conditions. Thermo gravimetric analysis (TGA) was carried out using a Perkin Elmer Pyris Diamond TG/DTA instrument by measuring their weight losses while heating at a rate of 10 °C/min. MALDI-TOF MS study was performed with DHB (2,5-dihydroxy benzoic acid) matrix by using Bruker UltrafleXtreme instrument. Scanning Electron Microscope (SEM) analysis was carried out with ZEISS MERLIN (GEMINI2) FESEM with Oxford EDS detector.

2. Synthesis and characterization

2a. Syntheses

2,5-Dibromo-3-methylthiophene[1] (1): To a solution of 3-methylthiophene (5.3 g, 53.9 mmol) in anhydrous THF (60 mL) was added a mixture of N-bromosuccimide (NBS) (24.2 g, 134.9 mmol) in THF (5 ml). The solution was stirred for 12 hours at 28 °C in the dark (by covering the flask with aluminum foil). After the reaction was completed (as monitored by TLC), distilled water was added. The organic phase was extracted from EtOAc (3 × 10 mL), washed with brine, dried over anhydrous $MgSO_4$. After filtration, the filtrate was concentrated under vacuum. The crude compound was purified by silica gel column chromatography (hexanes) to get a colourless oil (12.1 g, 87%). ^{1}H NMR (400 MHz, $CDCl_3$): δ 6.77 (s, 1H, thienyl), 2.15 (s, 3H, -CH_3). ^{13}C{^{1}H} NMR (100 MHz, $CDCl_3$): δ 138.2 (C, thiophene), 132.0 (CH, thiophene), 110.4 (C, thiophene), 108.7 (C, thiophene), 15.3 (-CH_3).

2,5-Dibromo-3-(bromomethyl)thiophene[1] (2): To a solution of 2,5-dibromo-3-methylthiophene (**1**) (4 g, 15.6 mmol) in anhydrous CCl_4 (40 mL), a mixture of N-bromosuccimide (NBS) (3.6 g, 20.3 mmol) and catalytic amount of AIBN was added. The solution was stirred for 22 hours at 80 °C in the dark (by covering the flask with aluminum foil). After the reaction was completed (as monitored by TLC), distilled water was added. The organic phase was extracted from EtOAc (3 × 10 mL), washed with brine solution, dried over anhydrous $MgSO_4$. It was then filtered, and the filtrate was concentrated under vacuum. The crude compound was purified by silica gel column chromatography (hexanes) to get a colourless oil (3.9 g, 76 %). ^{1}H NMR (400 MHz, $CDCl_3$): δ 7.00 (s, 1H, thienyl), 4.36 (s, 2H, -CH_2-Br). ^{13}C{^{1}H} NMR (100 MHz, $CDCl_3$): δ 138.0, 131.1, 112.4, 112.0 (aromatic carbons),

25.2 (-$\underline{C}H_2$-Br). MALDI-TOF (m/z): $C_5H_3Br_3S$, calculated value 333.748 $(M)^+$, found 333.653 $(M)^+$.

9-heptyl-3,6-bis(4,4,5,5-tetramethyl-1,3,2-dioxaborolan-2-yl)-9H-carbazole (**M1**): A solution of n-BuLi (1.6 M in hexanes, 9.3 mL, 14.8 mmol) was added dropwise to a solution of **6** (2.03 g, 4.8 mmol) in THF(50 mL) kept at -78 °C. The obtained mixture was vigorously stirred for 1 h at -78 °C before the addition of 2-isopropoxy-4,4,5,5-tetramethyl-[1,3,2]-dioxaborolane (3.8 g, 15.2 mmol) in one portion. The resulting solution was then allowed to reach room temperature and to react overnight. After removing the solvent under vacuum, CH_2Cl_2 (50 mL) was added and the obtained solution was washed with water (3 × 50 mL) and dried over anhydrous Na_2SO_4. The solvent was removed under vacuum and the obtained crude product was purified by flash column chromatography using silica gel (petroleum ether 40 - 60 °C and CH_2Cl_2, 1:1 v/v) to achive **M1** (1.7 g, 68%) as a white solid. ^{1}H NMR (400 MHz, $CDCl_3$): δ 8.67 (s, 2H, carbazolyl), 7.90 (d, 2H, *J* = 8 Hz, carbazolyl), 7.39 (d, 2H, *J* = 8 Hz, carbazolyl), 4.30 (t, 2H, *J* = 2 Hz, -N-C$\underline{H}_2$-), 1.88-1.83 (m, 2H, -N-CH_2-C$\underline{H}_2$-), 1.41-1.37 (m, 32H,-Me of O-Bpin, -CH_2- heptyl), 0.89-0.85 (m, 3H, -CH_3, heptyl). ^{13}C{^{1}H} NMR (100 MHz, $CDCl_3$): δ 142.7, 132.1, 128.0, 122.8, 108.1 (aromatic carbons), 83.5, 43.0, 31.7, 29.1, 28.9, 27.2, 26.3, 25.4, 24.9, 22.6, 21.0 (-CH_2-, heptyl), 14.2 (-CH_3, heptyl).

2,7-Bis(4,4,5,5-tetramethyl-1,3,2-dioxaborolan-2-yl)-9,9-dioctylfluorene (M2): In a 100 ml oven dried Schlenk flask purged with argon, compound **8** (1.64 g, 3.1 mmol) was dissolved in 25 mL of dry THF and it was brought to -78 °C. At this temperature ^{n}BuLi (4.6 mL of 1.6 M in n-hexane, 7.5 mmol) was added slowly through syringe over 15 min. It was stirred at this temperature for another 30 min. Then 2-isopropoxy-4,4,5,5- tetramethyl-1,3,2-dioxaborolane (2.06 g, 7.8 mmol) was added slowly through syringe over 10 min and stirred at -78°C for another 90 min. The reaction mixture was allowed to come 28 °C slowly and stirred for another 24h. Then the reaction was quenched by 3 mL of water. The compound was extracted from DCM and the organic layer was washed with brine solution followed by water, and dried over anhydrous MgSO4. The product was recrystallized from hexanes to obtain white crystalline solid. Yield: 1.5 g (78%); ^{1}H NMR (400 MHz, $CDCl_3$) δ 7.81-7.70 (m, 6H, fluorene), 2.01-1.97 (m, 4H, octyl protons), 1.38 (s, 24 H, -Me of O-Bpin), 1.19-1.00 (m, 20H, octyl), 0.80-0.78 (m, 4H, octyl), 0.56-0.53 (m, 6H, -Me octyl).; ^{13}C{^{1}H} NMR (100 MHz, $CDCl_3$) δ 150.7, 144.1, 133.9, 129.1, 119.6 (aromatic carbons), 83.9,55.4, 40.3, 32.0, 30.1, 29.4, 25.2, 22.8 (-CH_2-, octyl), 14.1 (-CH_3, octyl).

2,2'-(3-Hexylthiophene-2,5-diyl)bis(4,4,5,5-tetramethyl-1,3,2-dioxaborolane) (M3): In a 100 ml oven dried Schlenk flask purged with argon, compound **10** (1.1 g, 3.3 mmol) was dissolved in 25 mL of dry THF and it was brought to -78 °C. At this temperature ^{n}BuLi (4.6 mL of 1.6 M in n-hexane, 7.5 mmol) was added slowly through syringe over 15 min. It was stirred at this temperature for another 30 min. Then 2-isopropoxy-4,4,5,5- tetramethyl-1,3,2-dioxaborolane (2.2 g, 8.6 mmol) was added slowly through syringe over 10 min and stirred at -78 °C for another 90 min. The reaction mixture was allowed to come room temperature (28 °C) slowly and stirred for another 24h. Then the reaction was quenched by 3 mL of water. The compound was extracted in DCM and the organic layer was washed with brine solution followed by water, and dried over anhydrous $MgSO_4$. The product was obtained after concentration of the DCM solution, as light yellow oil. Yield: 1.0 g (78%); ^{1}H NMR (400 MHz, $CDCl_3$) δ 7.50 (s, 1H, thienyl), 2.86 (t, 2H, hexyl protons), 1.61-1.56 (m, 8H, hexyl protons), 1.39-1.31(s, 24 H, -Me of -O-Bpin), 0.90-0.86 (m, 3H, hexyl).^{13}C{^{1}H} NMR (100 MHz, $CDCl_3$): δ 145.7, 141.1, 127.0, 125.8, 108.1 (aromatic carbons), 55.6, 43.0, 31.7, 25.4, 24.9, 22.6, 21.0 (-CH_2-, hexyl), 14.3 (-CH_3, hexyl).

Hydroxyapatite [HAP, $Ca_{10}(PO_4)_6(OH)_2$][2]: $Ca(NO_3)_2$. $4H_2O$ (15.0 g, 0.066 mol) dissolved in water (60 mL) was brought to pH 11-12 with concentrated NH_4OH and thereafter diluted to 120 mL. A solution of $(NH_4)_2HPO_4$ (5.28 g, 0.04 mol) in 100 mL water was brought to pH 11-12 with concentrated NH_4OH and thereafter diluted to 160 mL. The calcium solution was vigorously stirred at room temperature, and the phosphate solution was added drop wise over a period of 30 min to produce a milky and gelatinous precipitate which was then stirred and boiled for 10 min. The precipitate was filtered, washed, dried at 80 ºC overnight and calcined at 500 ºC for 3 h. All the synthetic steps were carried out using doubly distilled water.

Preparation of Copper(II)-hydroxyapatite (Cu-HAP)[2]: A calcium hydroxyapatite (2.0 mmol) sample of Ca/P = 1.67 [$Ca_{10}(PO_4)_6(OH)_2$] (HAP) was stirred with $Cu(NO_3)_2$ (0.20 mmol) in H_2O (150 mL) at 70 °C for 24 h. The obtained slurry was filtered, washed with deionized water, and dried overnight at 110 °C to afford a Cu(II)-exchanged hydroxyapatite (CuHAP, Cu content: 0.10 mmol g^{-1}) as a blue powder. No Cu(II) was detected in the filtrate or in the washing water. Thus, the Cu content can be estimated to be the same molar amount as that of $Cu(NO_3)_2$ used.

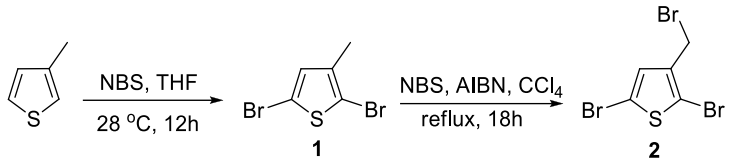

Scheme S1: Synthesis of 2,5-dibromo-3-bromomethyl thiophene from 3-methylthiophene.

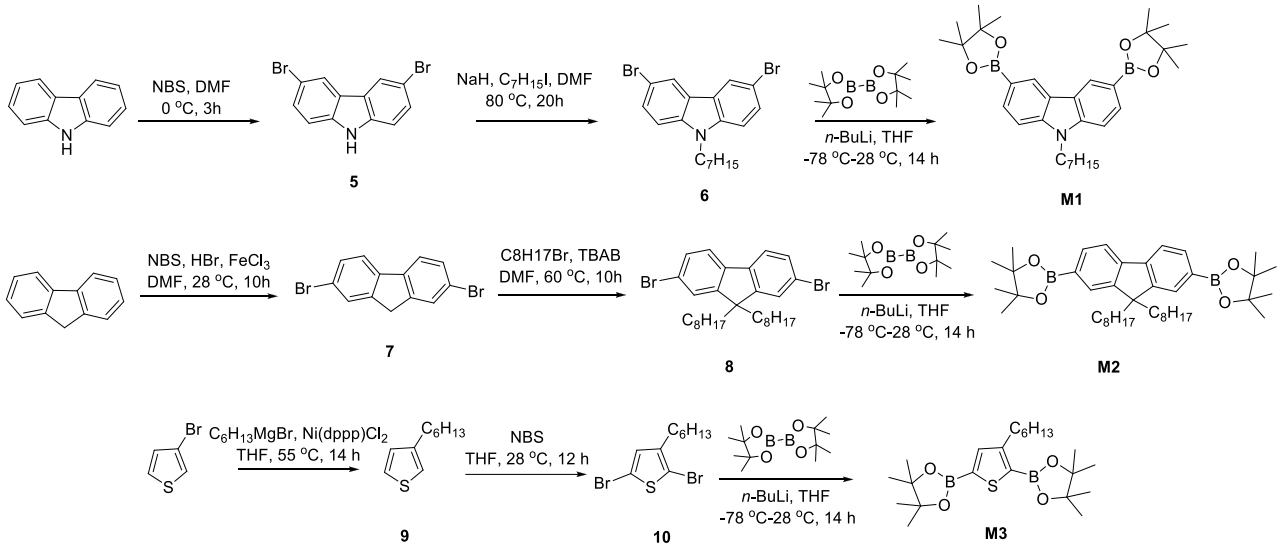

Scheme S2: Synthetic scheme for the key precursors and the monomers **M1, M2 and M3.**

2b. NMR Spectra

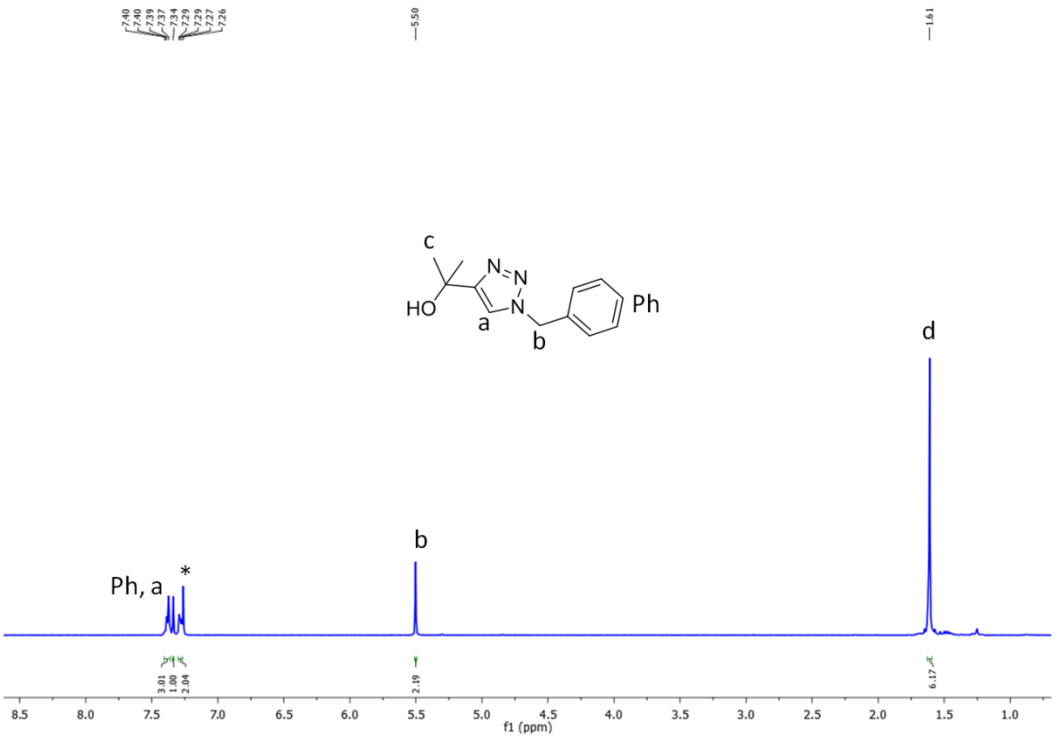

Figure S1a: ^{1}H NMR (400 MHz, $CDCl_3$) spectrum of **3.**

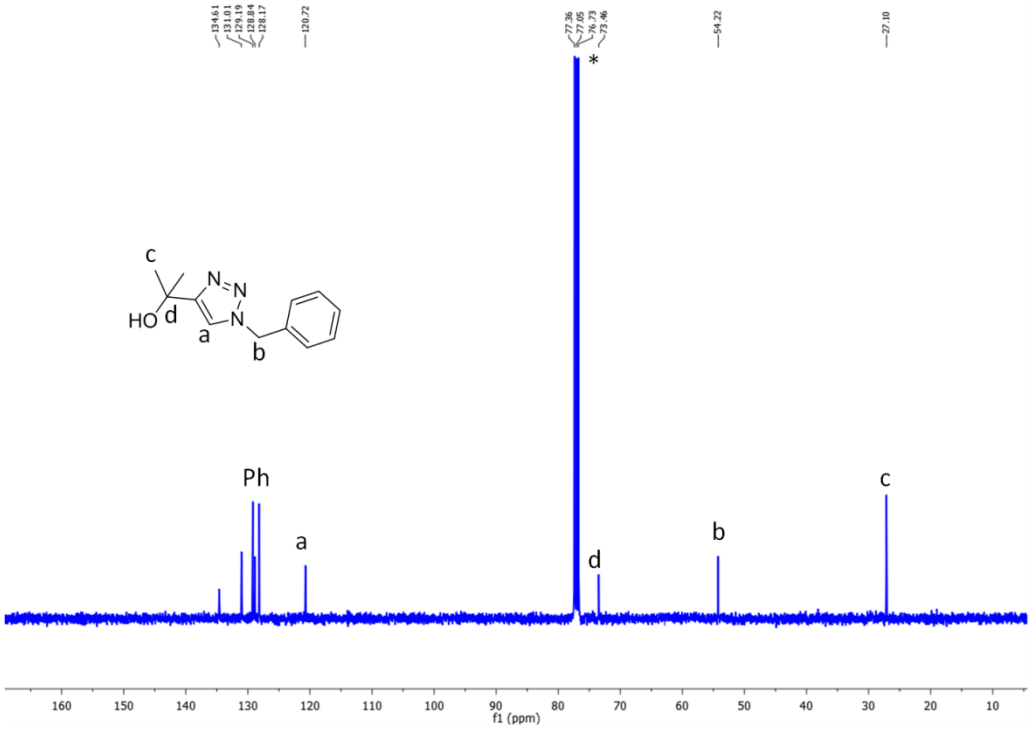

Figure S1b: $^{13}C\{^{1}H\}$ NMR (100 MHz, $CDCl_3$) spectrum of **3.**

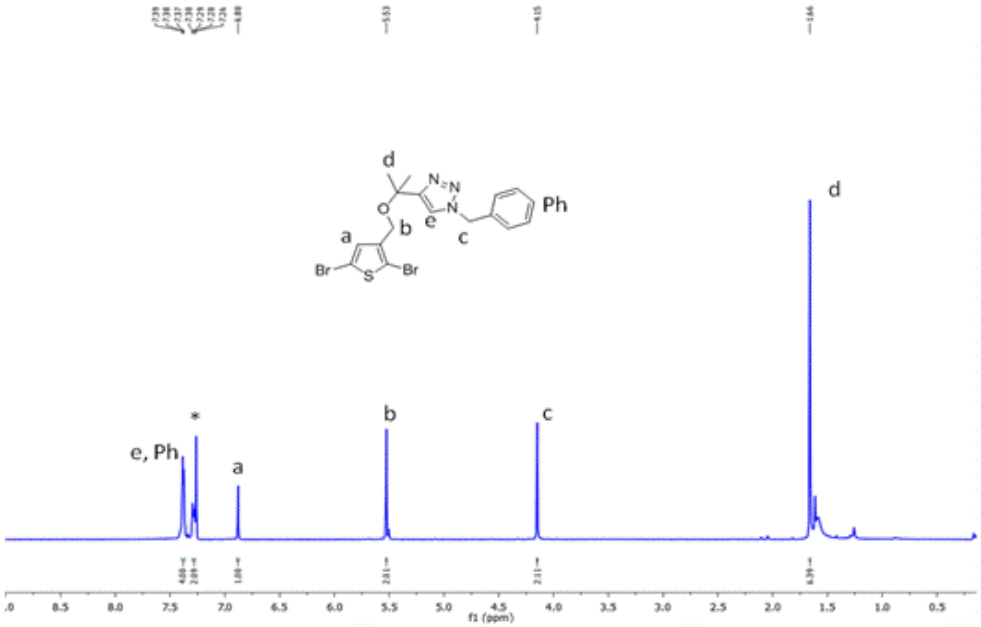

Figure S2a: ^{1}H NMR (400 MHz, $CDCl_3$) spectrum of **4.**

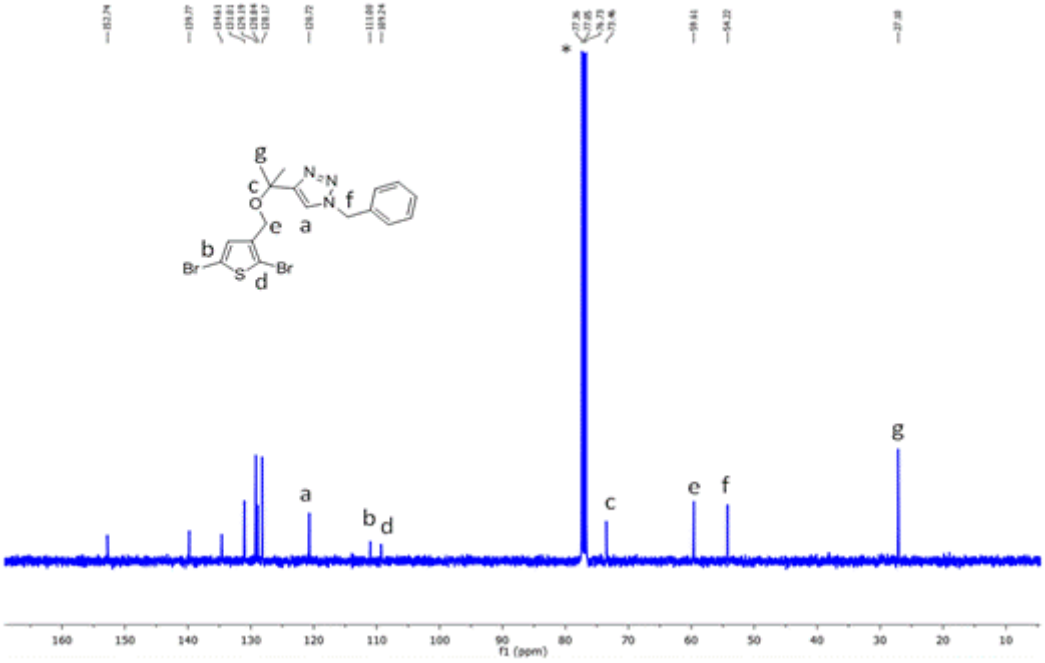

Figure 2b: $^{13}C\{^{1}H\}$ NMR (100 MHz, $CDCl_3$) spectrum of **4.**

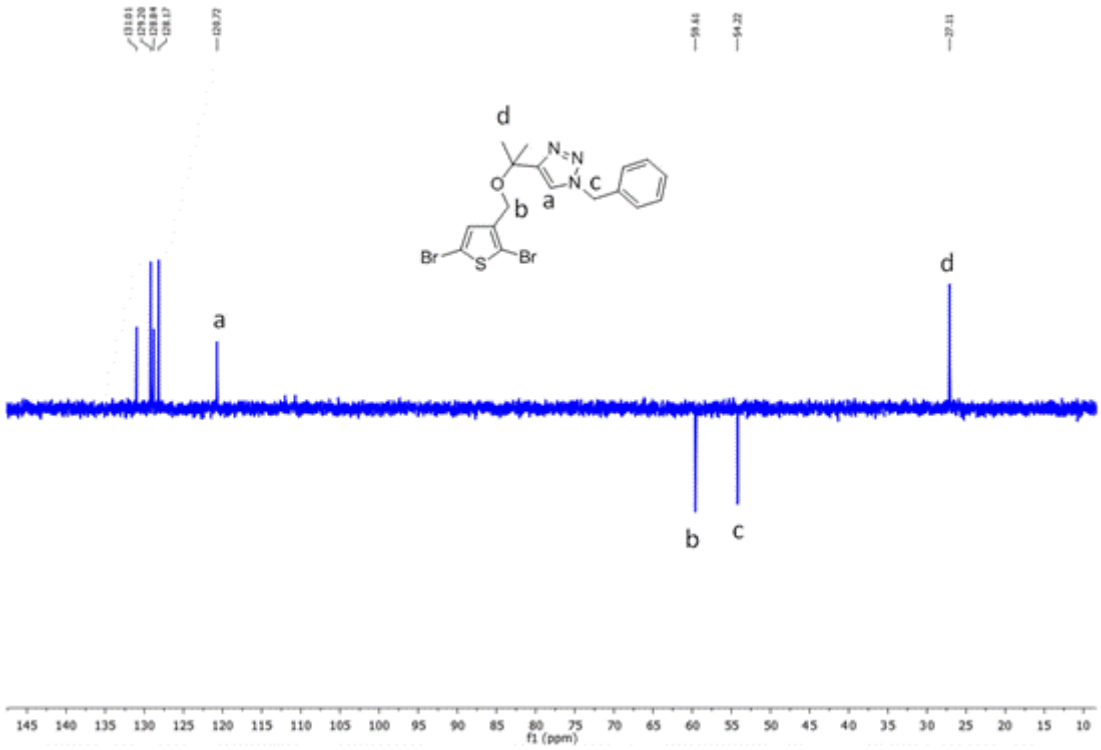

Figure S2c: DEPT-135(100 MHz, $CDCl_3$) spectrum of **4.**

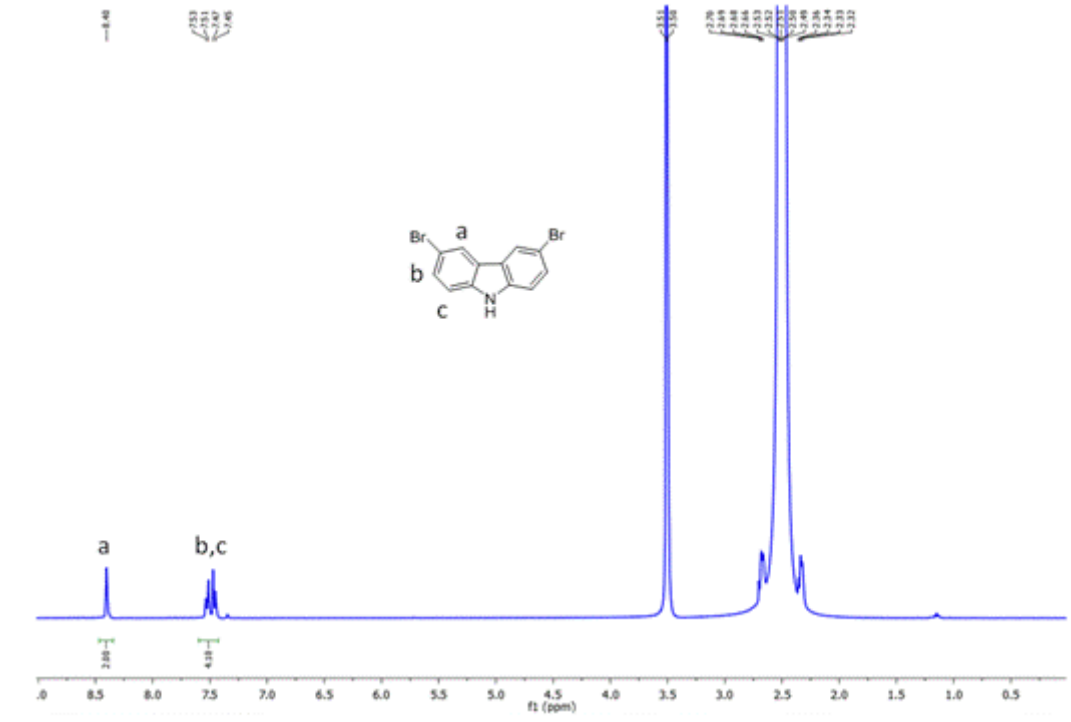

Figure S3a: ^{1}H NMR (400 MHz, DMSO-D_6) spectrum of **5.**

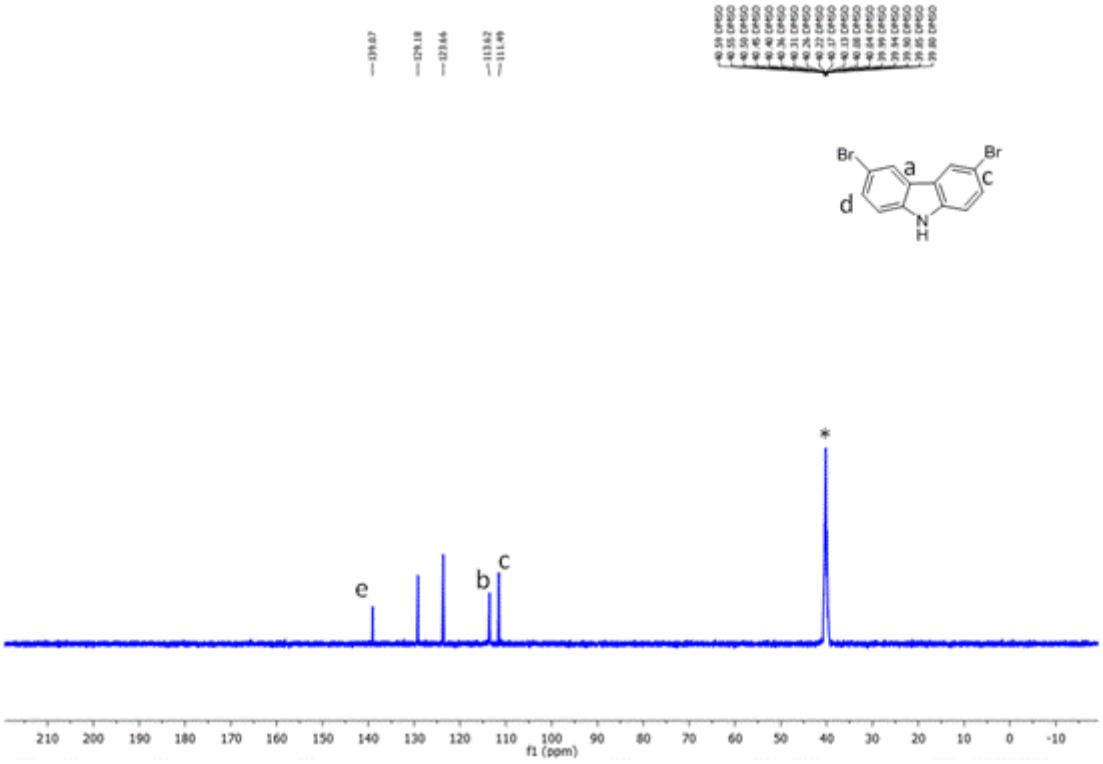

Figure S3b: $^{13}C\{^{1}H\}$ NMR (100 MHz, DMSO-D_6) spectrum of **5.**

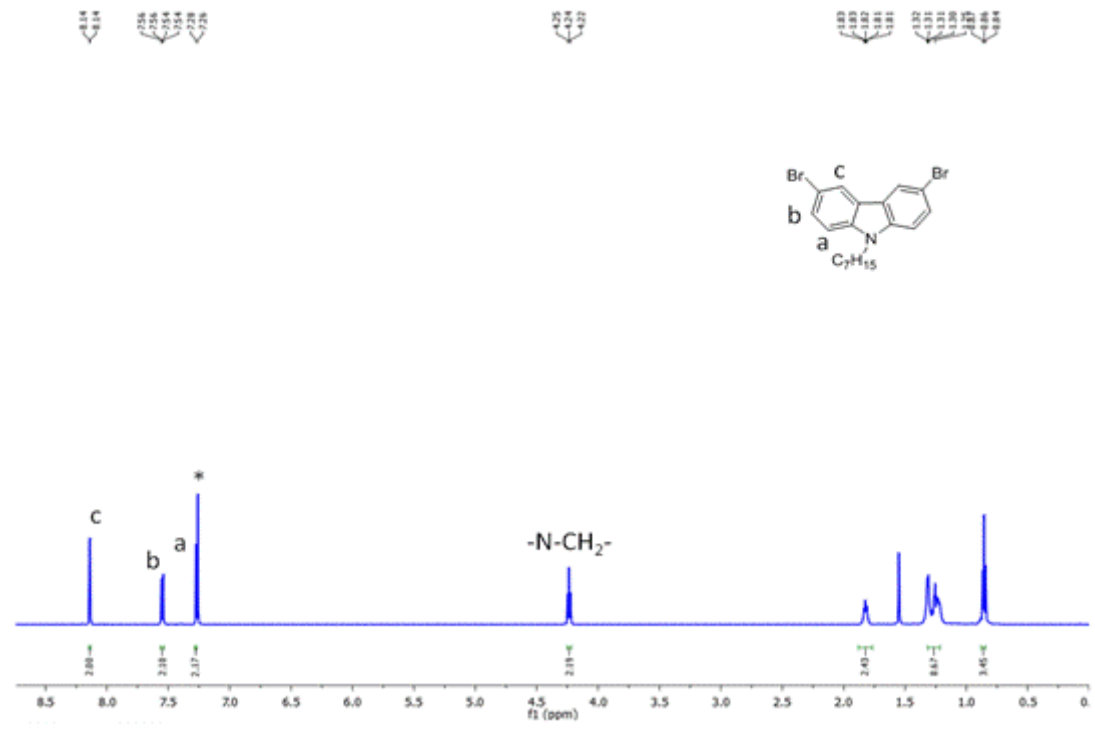

Figure S4a: ^{1}H NMR (400 MHz, $CDCl_3$) spectrum of **6.**

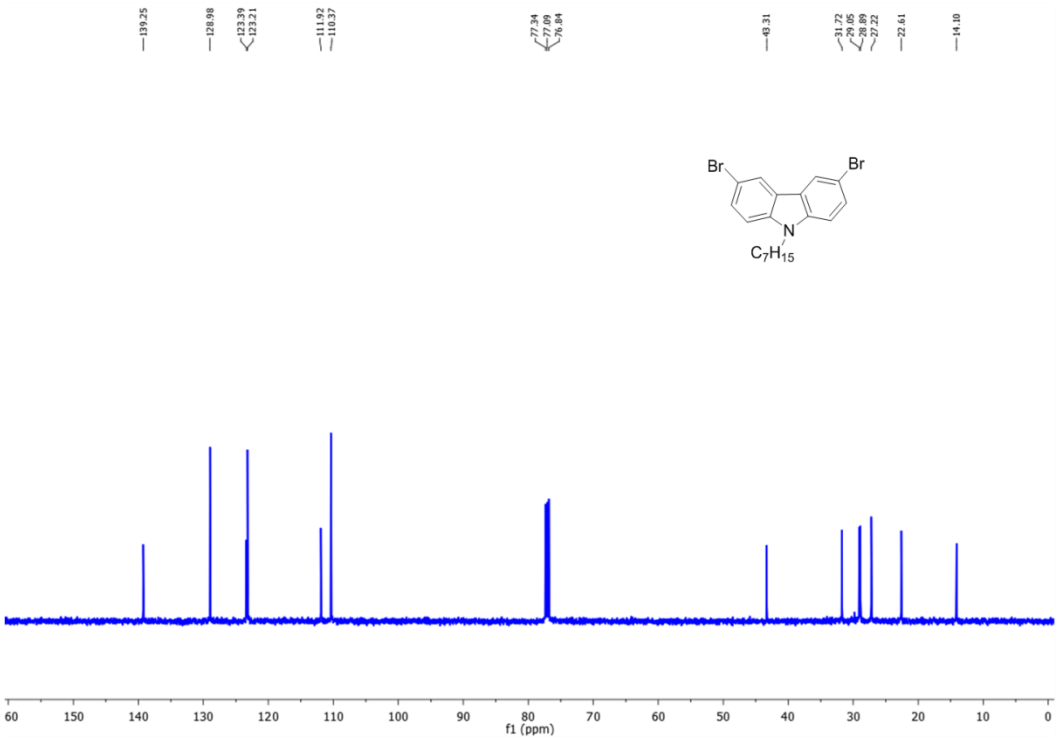

Figure S4b: $^{13}C\{^{1}H\}$ NMR (100 MHz, $CDCl_3$) spectrum of **6.**

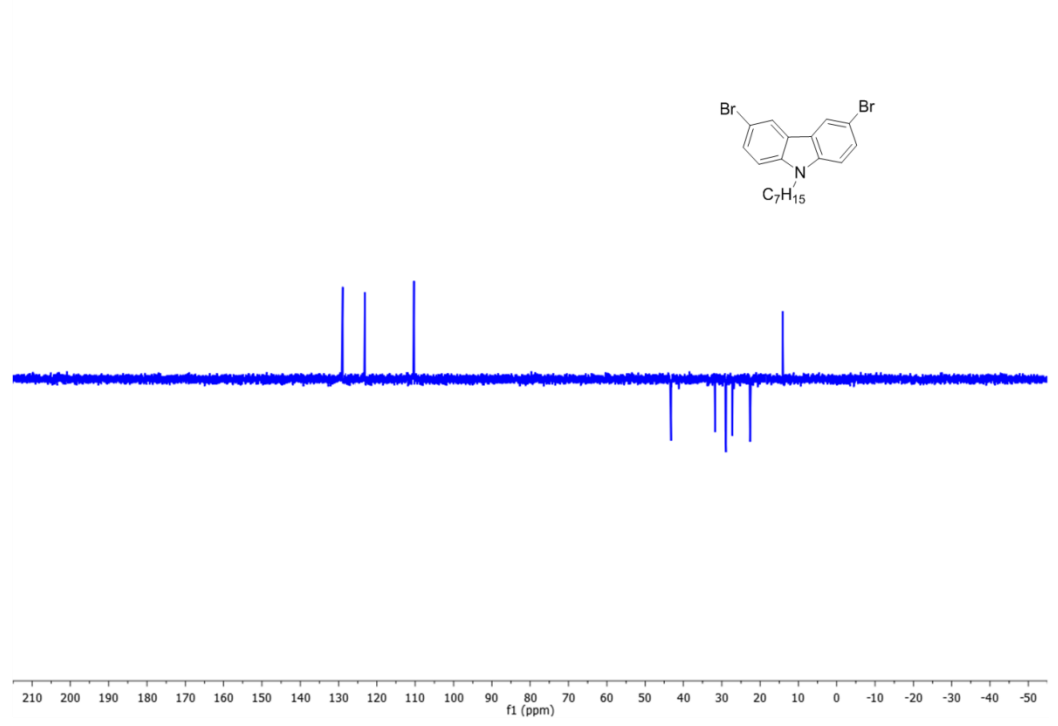

Figure S4c: DEPT-135 (100 MHz, $CDCl_3$) spectrum of **6.**

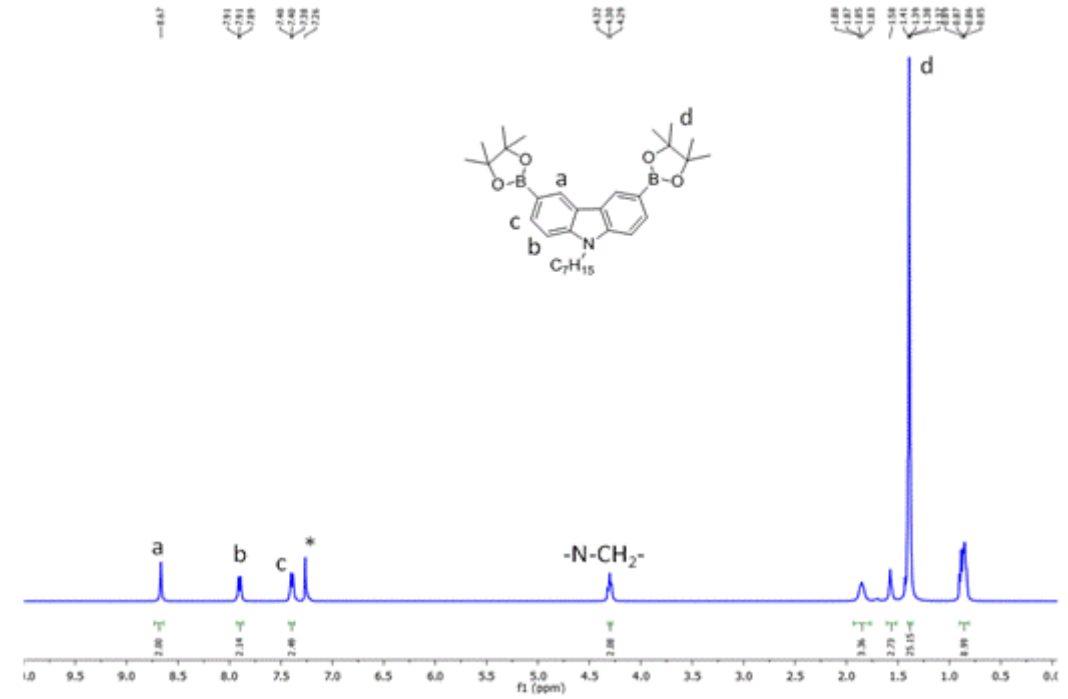

Figure S5a: ^{1}H NMR (400 MHz, $CDCl_3$) spectrum of **M1.**

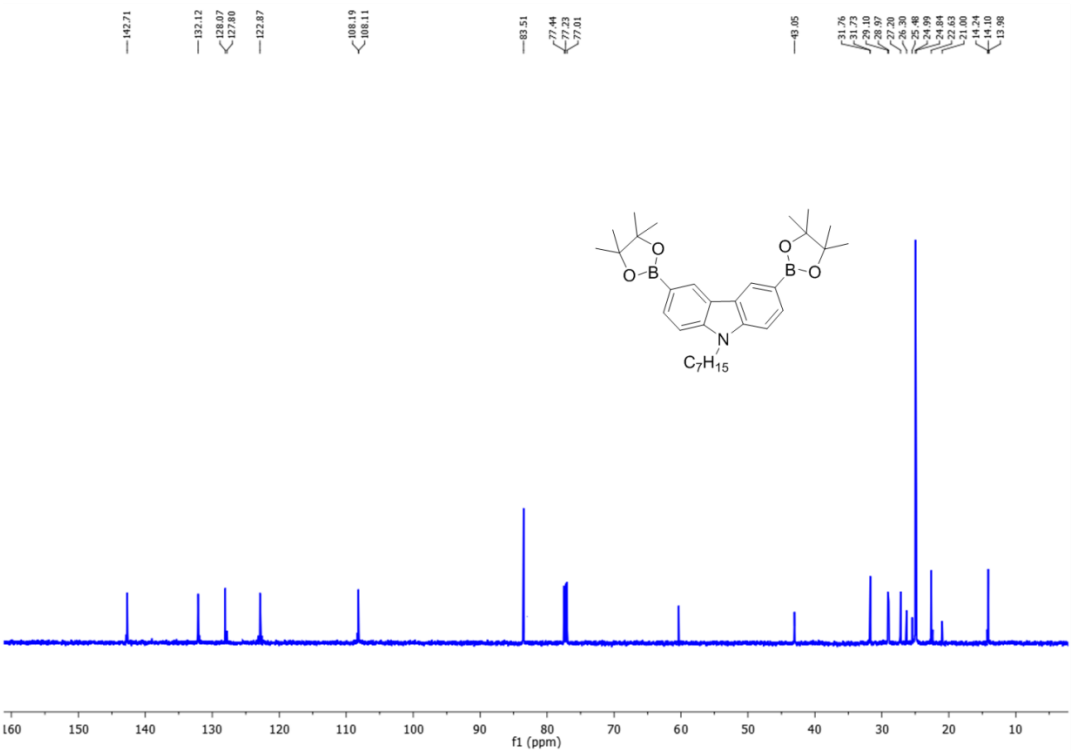

Figure S5b: $^{13}C\{^{1}H\}$ NMR (100 MHz, $CDCl_3$) spectrum of **M1.**

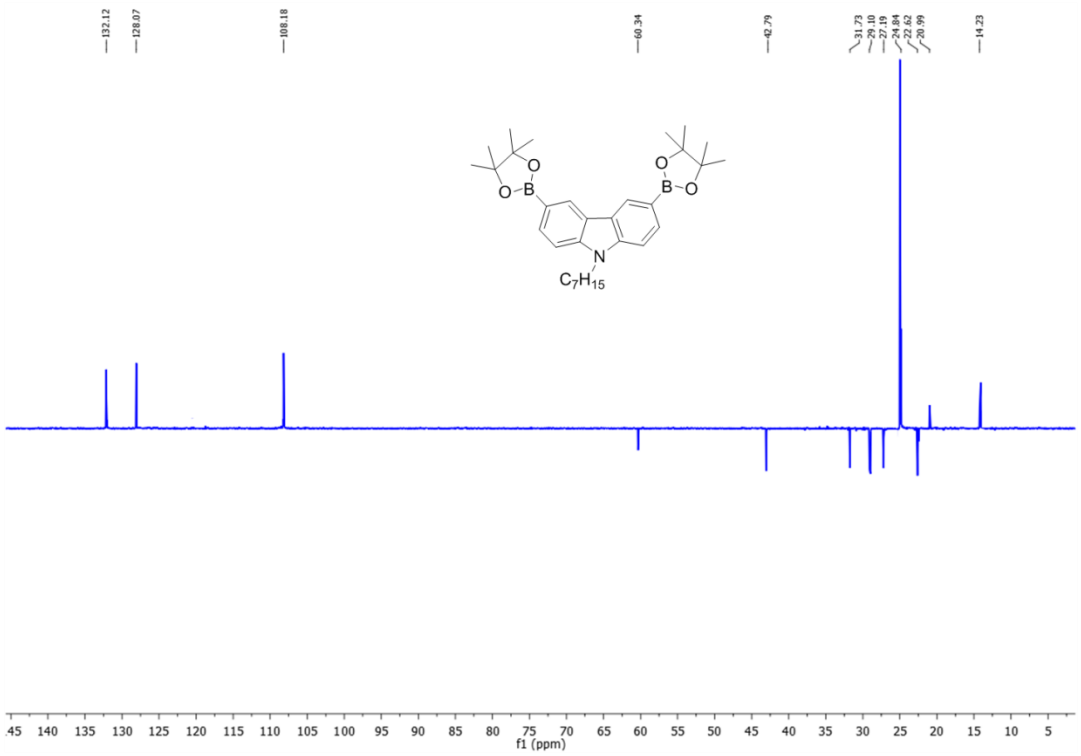

Figure S5c: DEPT-135 (100 MHz, $CDCl_3$) spectrum of **M1.**

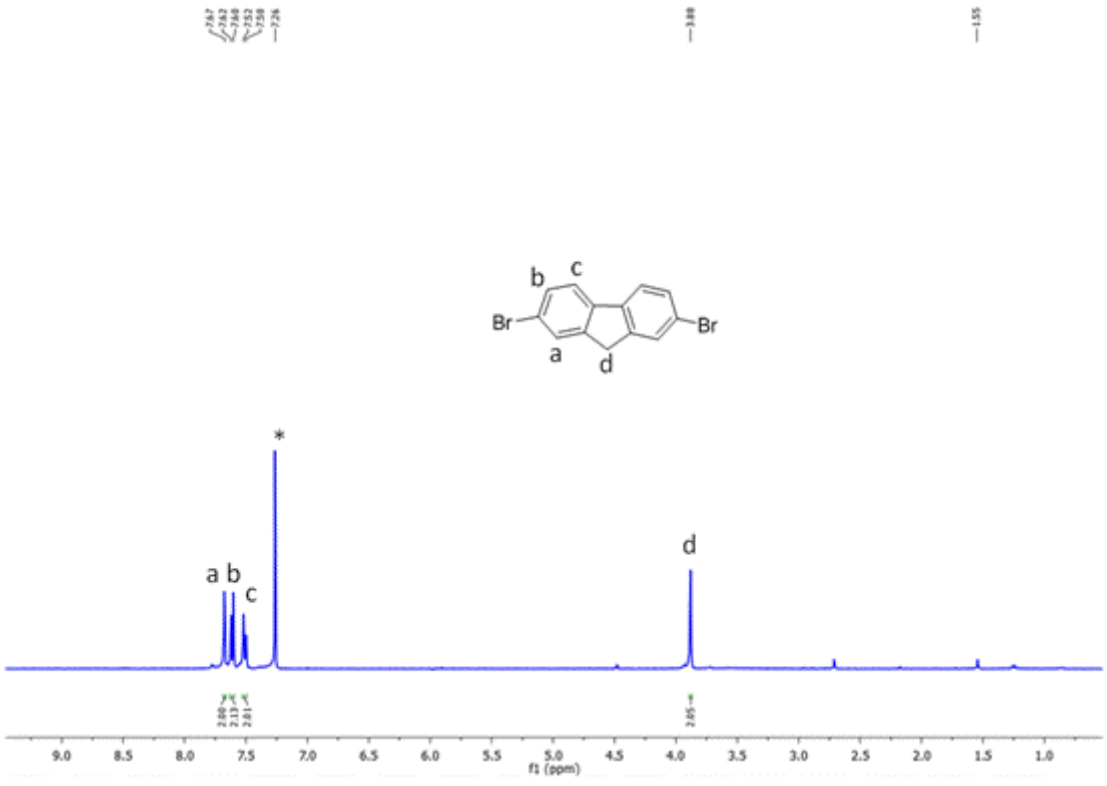

Figure S6a: ^1H NMR (400 MHz, $CDCl_3$) spectrum of **7.**

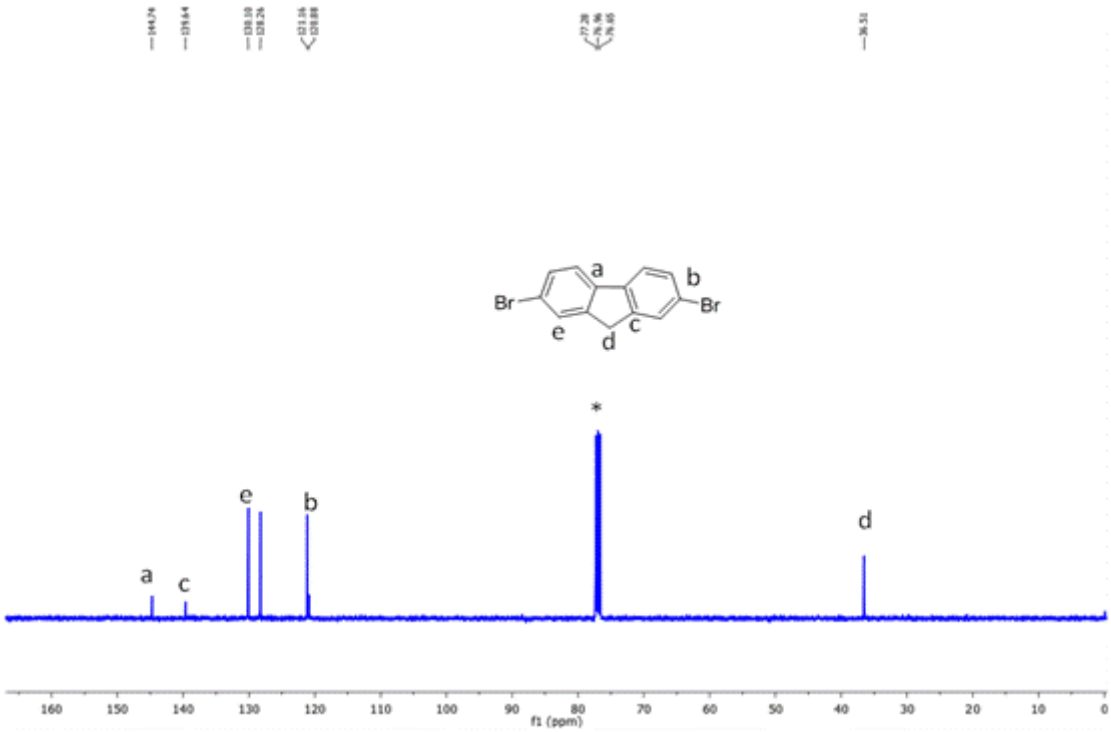

Figure S6b: $^{13}C\{^{1}H\}$ NMR (100 MHz, $CDCl_3$) spectrum of **7.**

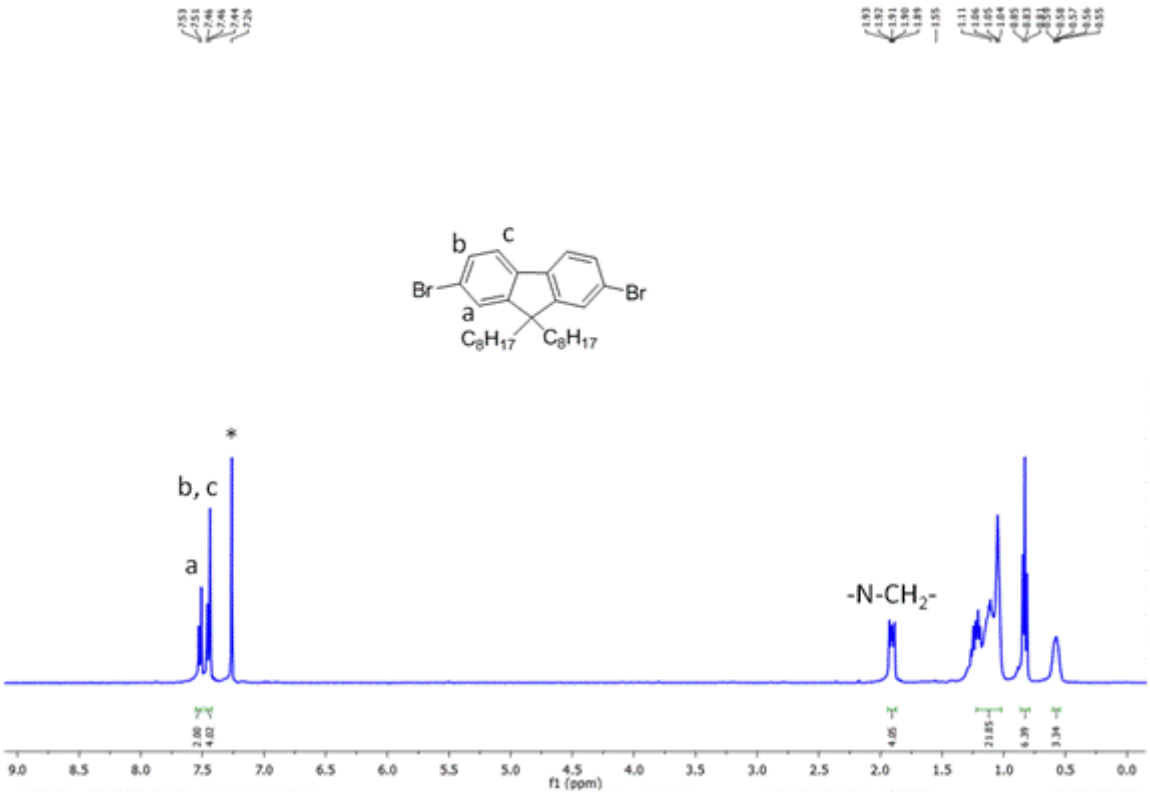

Figure S7a: ^{1}H NMR (400 MHz, $CDCl_3$) spectrum of **8.**

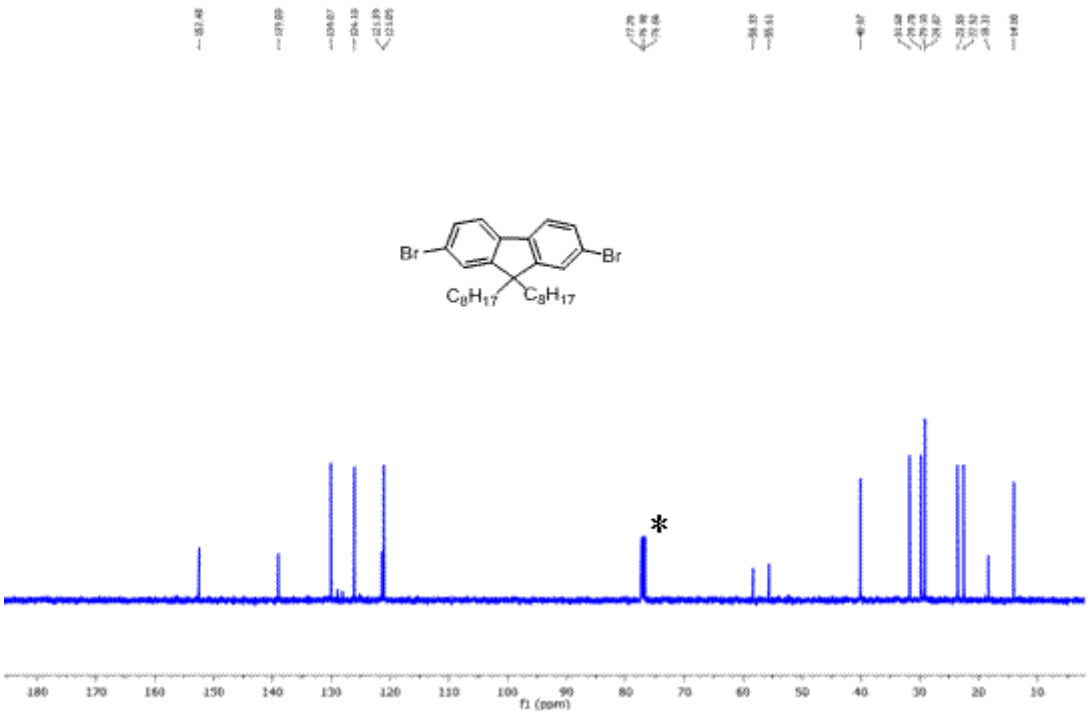

Figure S7b: $^{13}C\{^{1}H\}$ NMR (100 MHz, $CDCl_3$) spectrum of **8.**

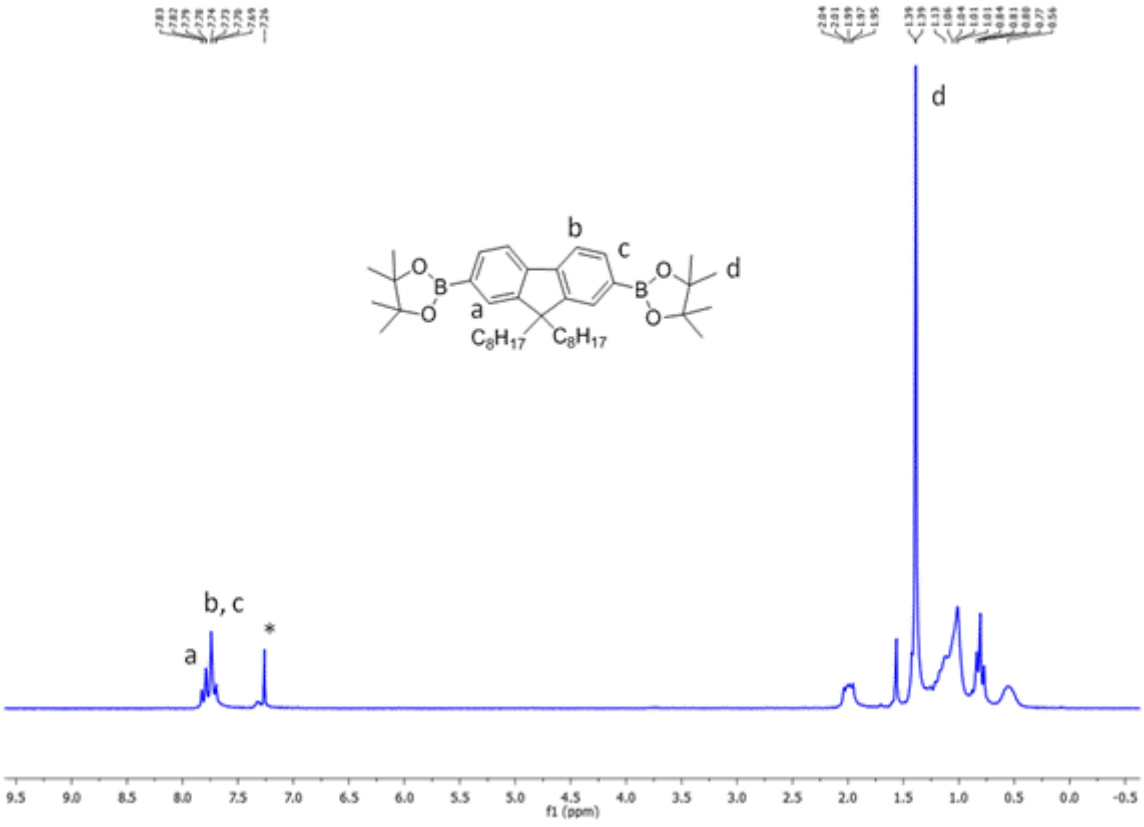

Figure S8a: ^{1}H NMR (500 MHz, $CDCl_3$) spectrum of **M2.**

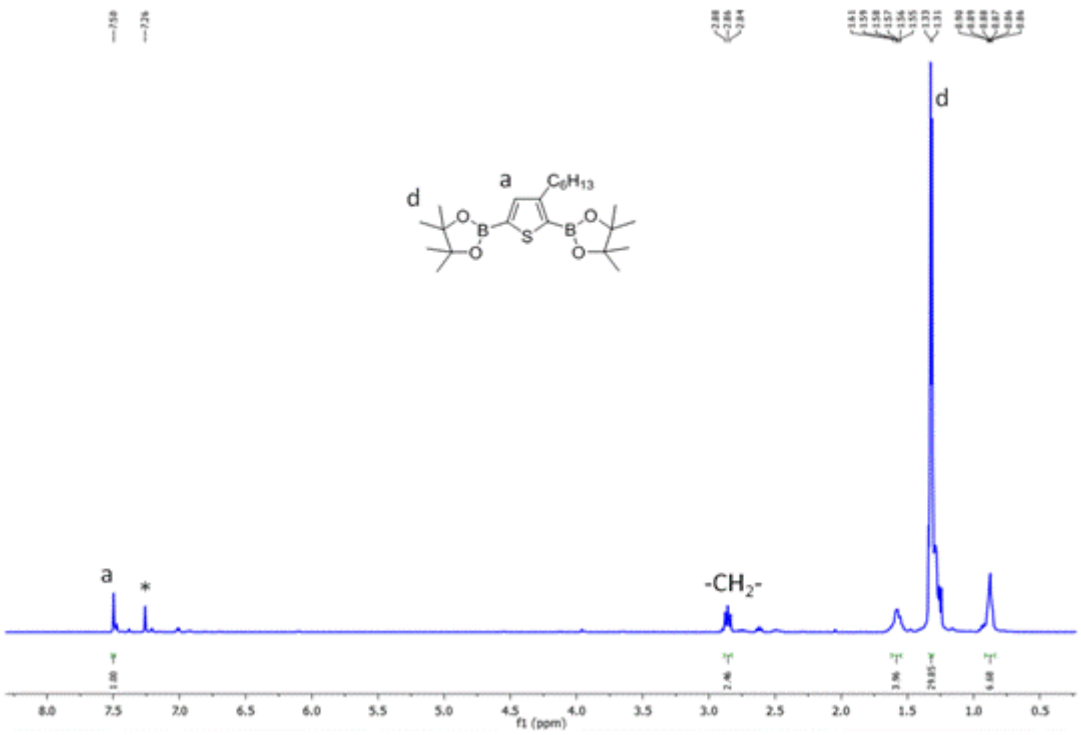

Figure S9a: ^{1}H NMR (500 MHz, $CDCl_3$) spectrum of **M3.**

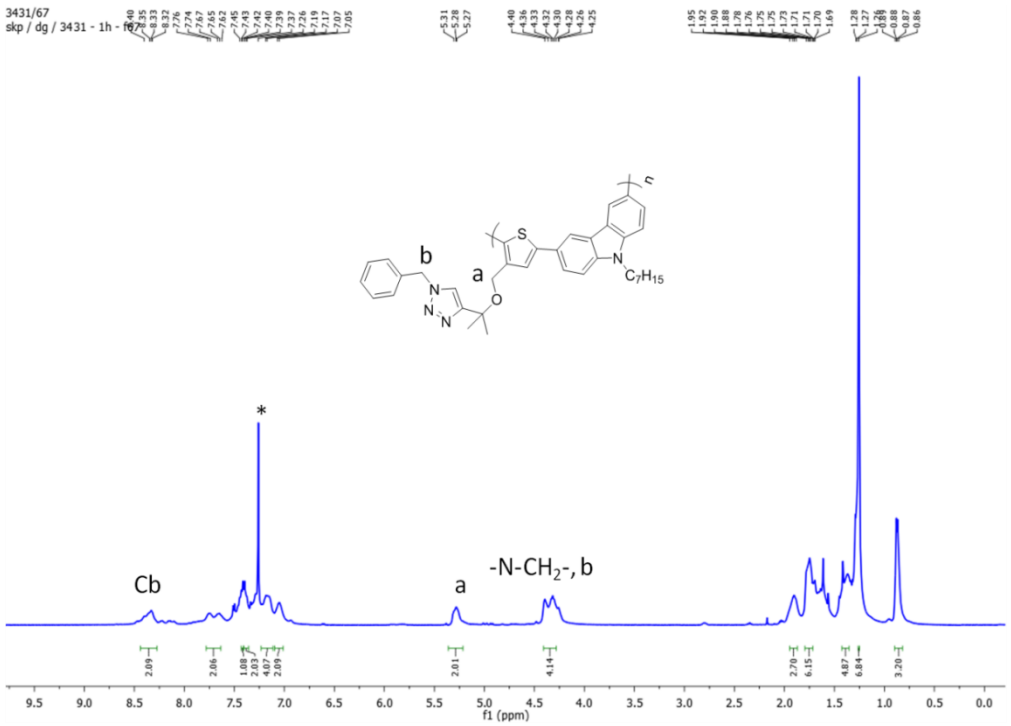

Figure S10a: ^{1}H NMR (600 MHz, $CDCl_3$) spectrum of **P1.**

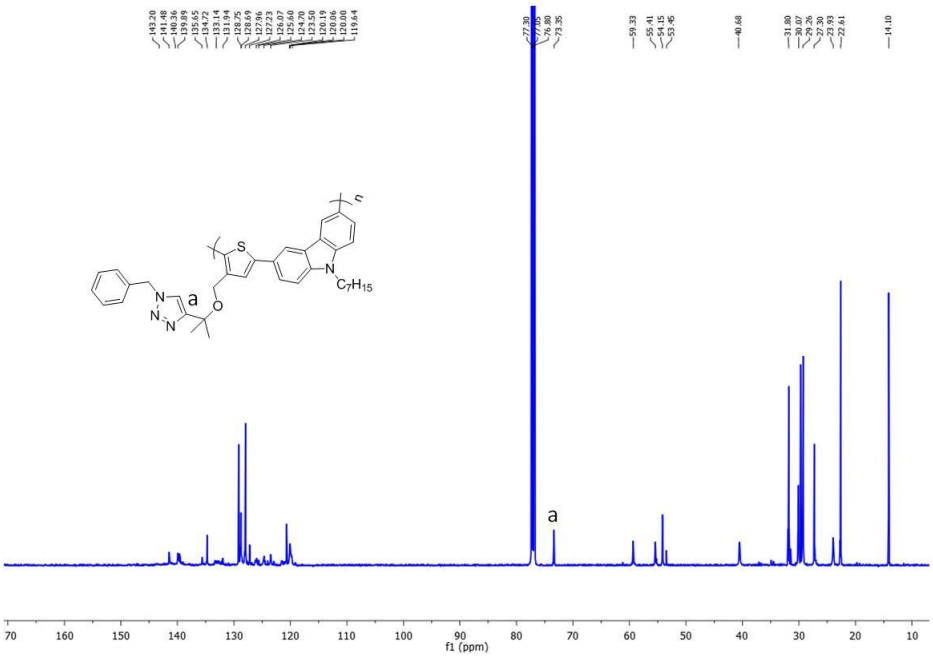

Figure S10b: $^{13}C\{^{1}H\}$ NMR (100 MHz, $CDCl_3$) spectrum of **P1.**

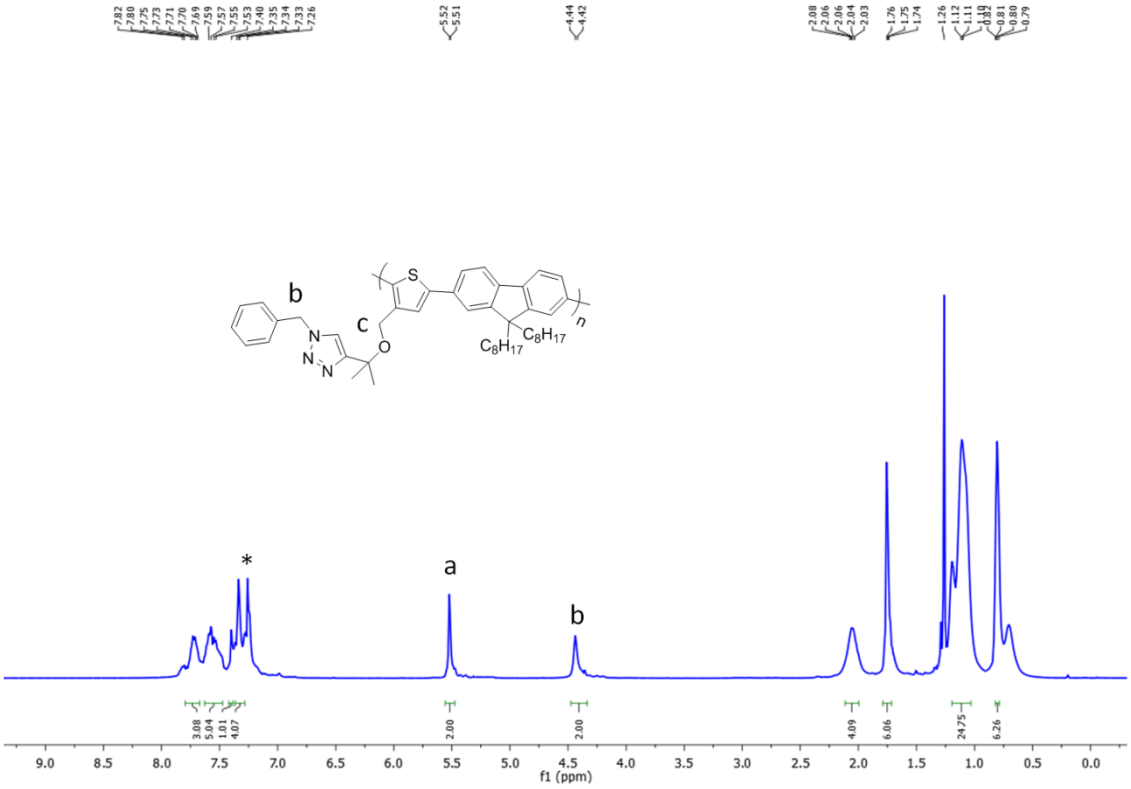

Figure S11a: ^{1}H NMR (600 MHz, $CDCl_3$) spectrum of **P2.**

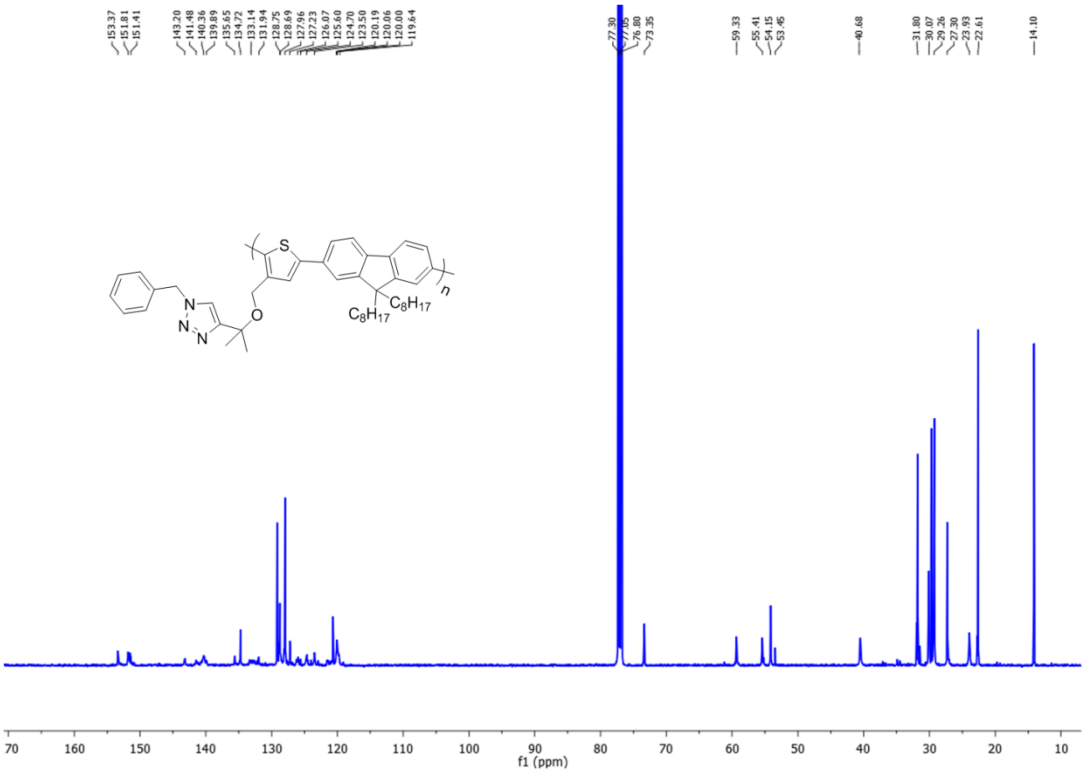

Figure S11b: $^{13}C\{^{1}H\}$ NMR (100 MHz, $CDCl_3$) spectrum of **P2.**

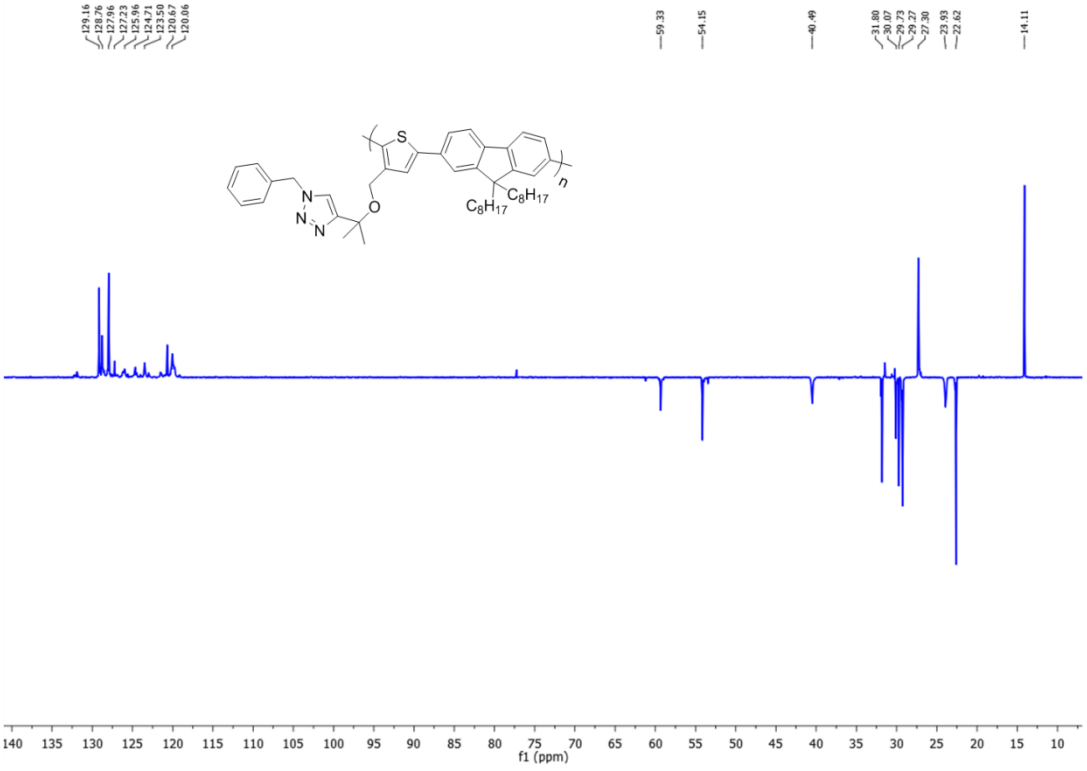

Figure S11c: DEPT-135 (100 MHz, $CDCl_3$) spectrum of **P2.**

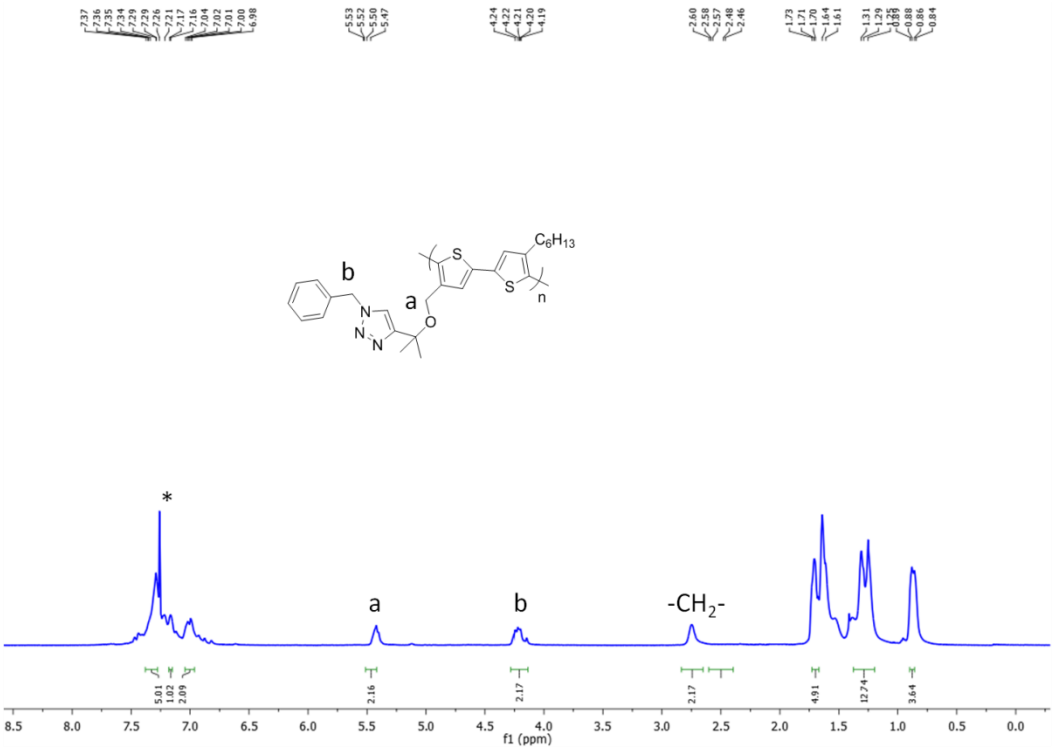

Figure S12a: ^{1}H NMR (600 MHz, $CDCl_3$) spectrum of **P3.**

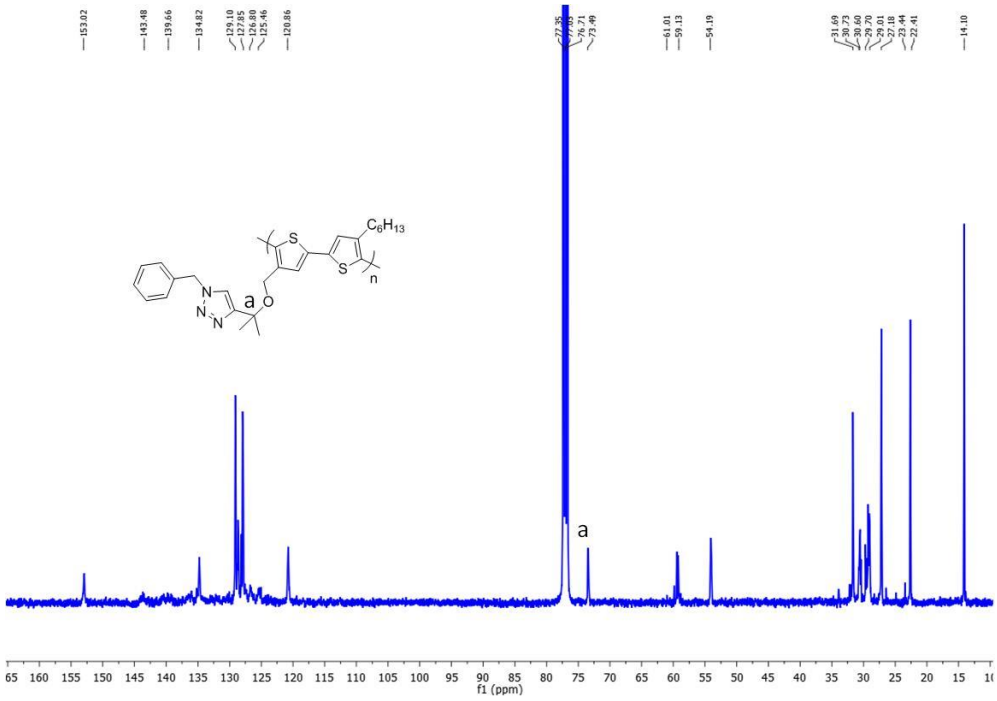

Figure S12b: $^{13}C\{^{1}H\}$ NMR (100 MHz, $CDCl_3$) spectrum of **P3.**

2c. Mass spectrometry

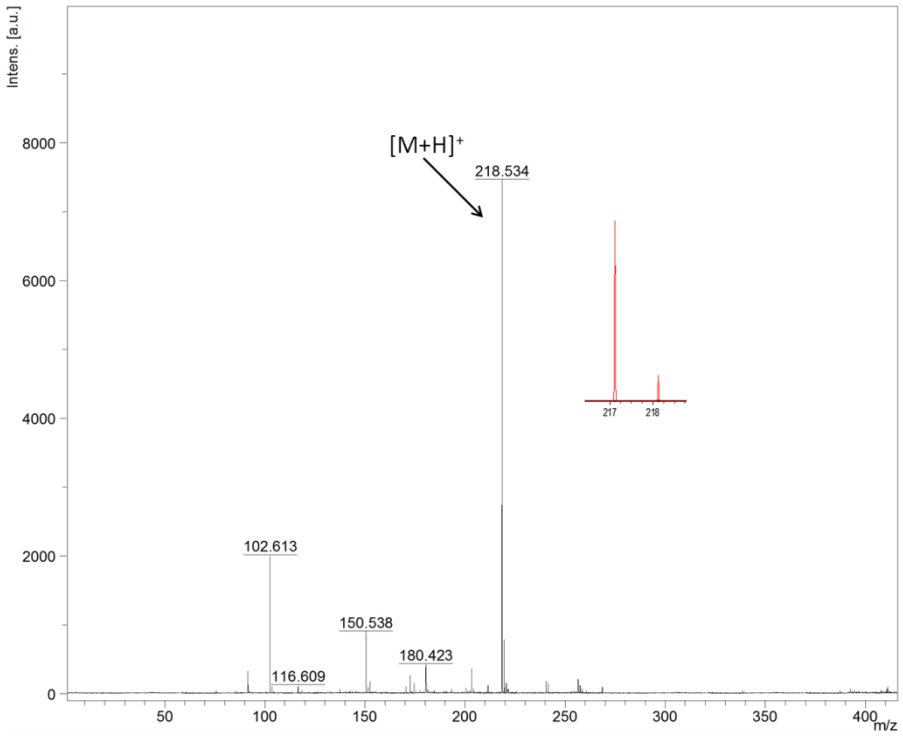

Figure S13: MALDI-TOF MS of **3**

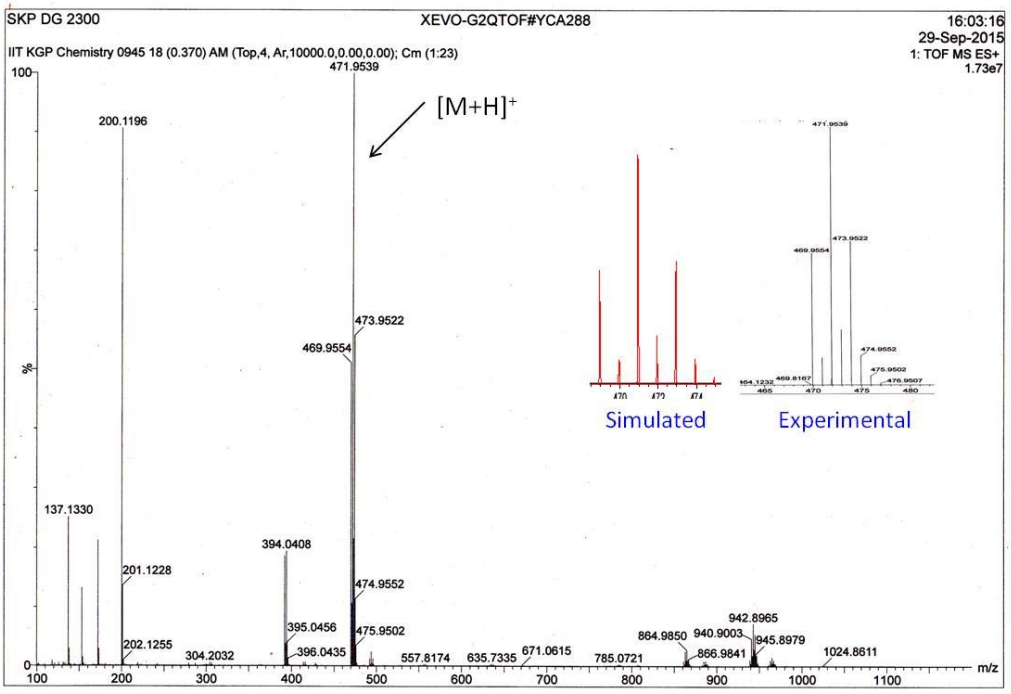

Figure S14: HRMS of **4.**

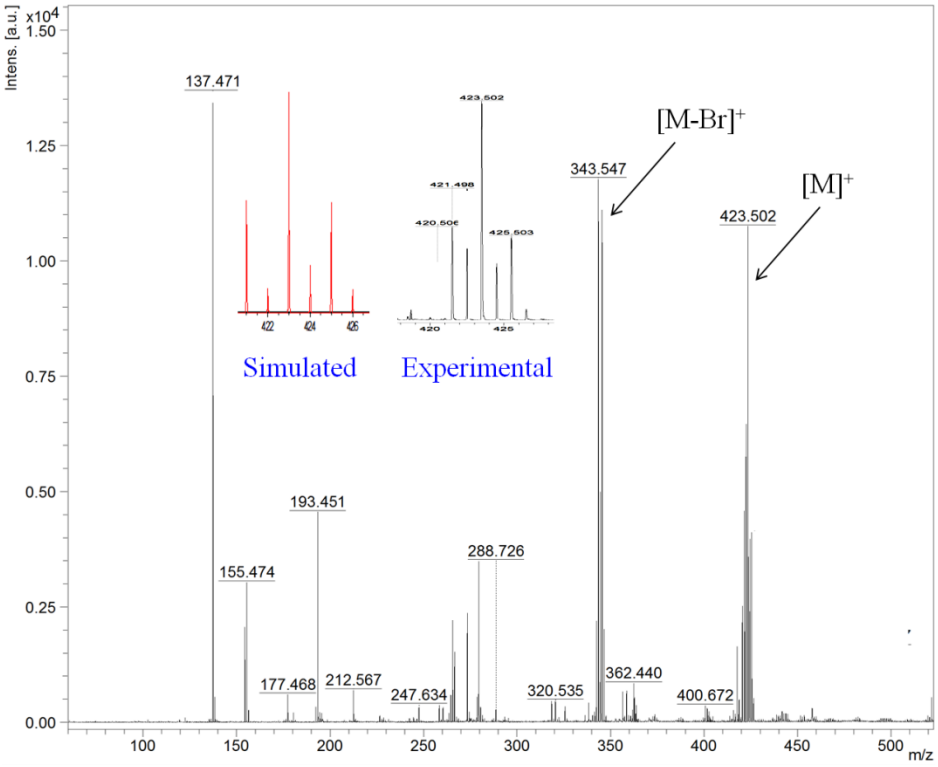

Figure S15: MALDI-TOF MS of **6**

2d. FT-IR spectrum (measured as KBr pellets**)**

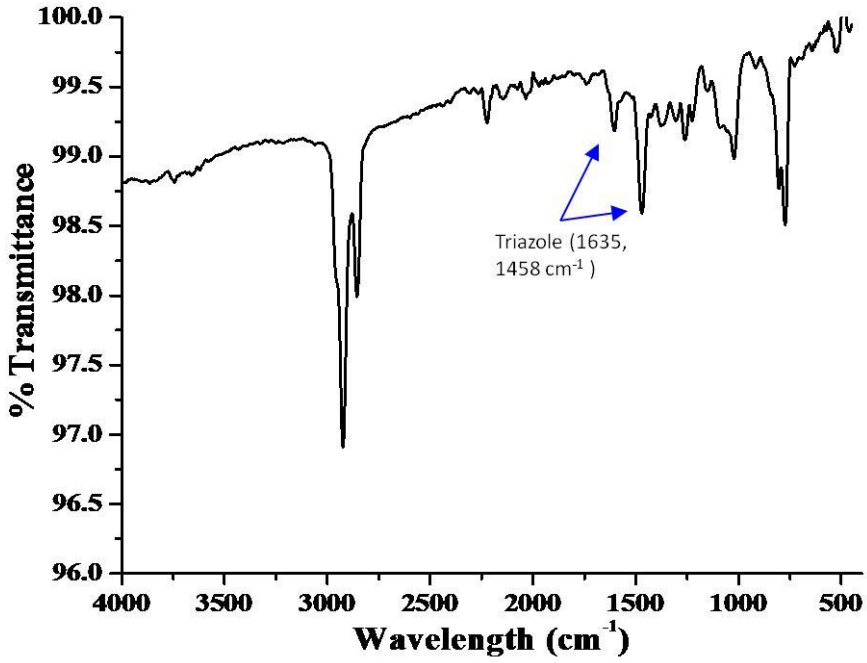

Figure S16a: FT-IR spectrum of **P1.**

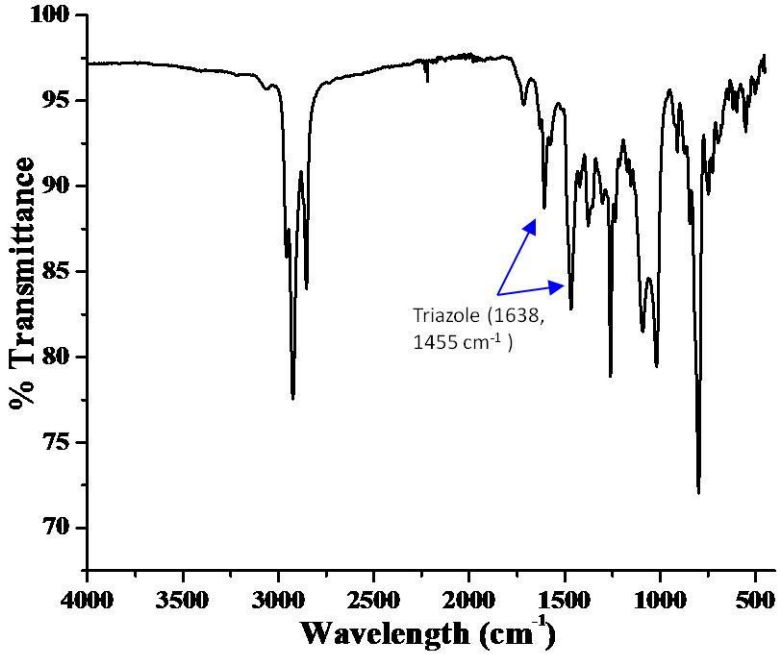

Figure S16b: FT-IR spectrum of **P2.**

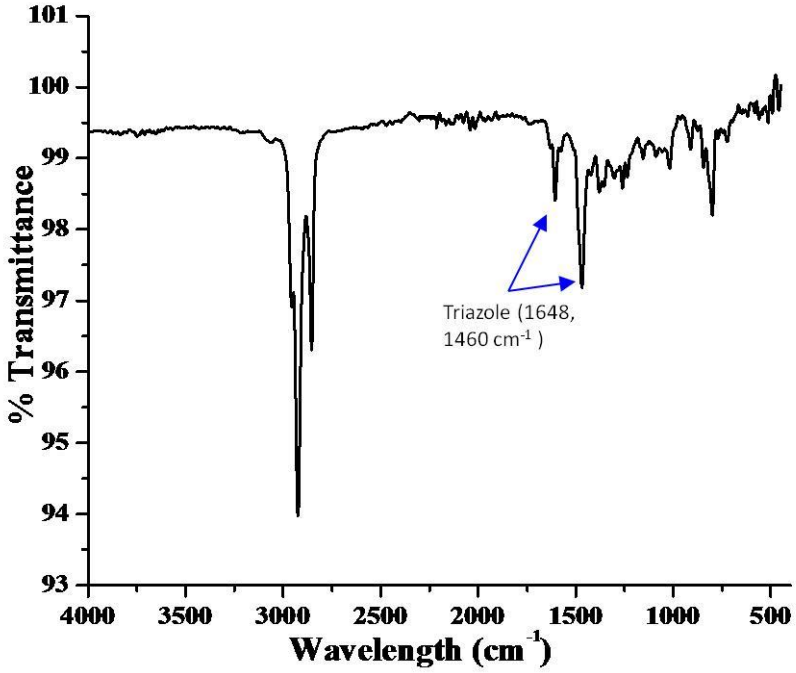

Figure S16c: FT-IR spectrum of **P3.**

2e. Thermal studies

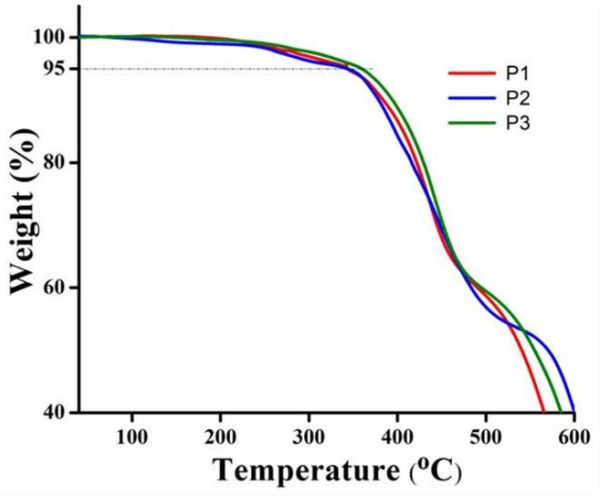

Figure S17: TGA thermograms of the polymers (**P1-P3**) recorded at a rate of 10 °C/min under N_2.

3. Photophysical and Sensing studies

3a. Determination of quantum yield

All the UV−Vis absorption and fluorescence emission spectra were collected using a Shimadzu (model UV 2450) UV−Vis spectrophotometer and a Spex Fluorolog-3 (model FL3−11) spectrofluorimeter, respectively. Throughout all the measurements, the concentration was maintained at ~1×10^{-5} M. Fluorescence quantum yields were measured with respect to a secondary standard quinine sulphate (λ_{abs}=350 nm) in 0.1 M H_2SO_4 (Φ = 0.54) at 298 K[3].The following equation was used to calculate the quantum yields:

$$\frac{\boldsymbol{\Phi_S}}{\boldsymbol{\Phi_R}} = \frac{\boldsymbol{A_S}}{\boldsymbol{A_R}} \times \frac{(\boldsymbol{Abs})_R}{(\boldsymbol{Abs})_S} \times \frac{\boldsymbol{\eta_S^2}}{\boldsymbol{\eta_R^2}} \text{.....(1)}$$

Here Φ represents the quantum yield, (Abs) represents the absorbance, A represents the area under the fluorescence curve, and η is the refractive index of the medium. η_{CHCl3} was calculated using Arago-biot (AB) equation.[3] The subscript S and R denotes the corresponding parameters for the sample and reference, respectively.

3b. Experimental details and determination of time resolved fluorescence spectra

The time-resolved emission decays were recorded using a Time-Correlated Single Photon Counting (TCSPC) picoseconds spectrophotometer. The fluorescence decay response of **P1, P2** and **P3**, and with incremental addition of picric acid was investigated in $CHCl_3$. The solution of picric acid was prepared in $CHCl_3$ and was added to the stock solution of **P1, P2**

and **P3**, which were prepared in $CHCl_3$. All the samples were excited using a picosecond diode laser at 400 nm (IBH, UK, Nanoled), and the signals were recorded at magic angle (54.71) using a Hamamatsu micro channel plate photomultiplier tube (3809U). The typical instrument response function in our setup is 100 ps. The instrument response function of our setup is ~800 ps. Time-resolved fluorescence decays were analyzed using IBH DAS-6 decay analysis software.

Table S1: Time resolved fluorescence data of **P1, P2** and **P3**

Polymer	τ_1 (ns)	τ_2 (ns)	α_1	α_2	τ_{av} (ns)
P1	0.32	0.53	0.72	0.28	0.38
P2	0.23	0.42	0.36	0.64	0.30
P3	0.28	0.62	0.32	0.68	0.36

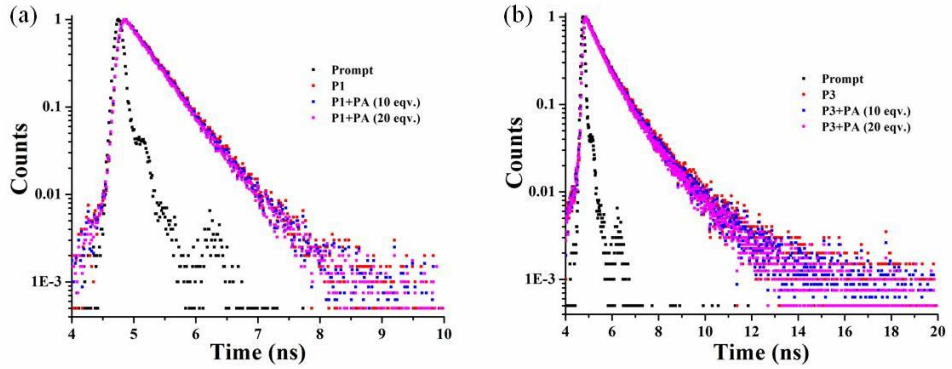

Figure S18: Fluorescence life time decay of (a) free **P1** and **P1** in presence of picric acid (10 and 20 eqv.), (b) free **P3** and **P3**in presence of picric acid (10 and 20 eqv.).

3c. Concentration dependent fluorescence study

Polymer concentrations were calculated as per the molecular weight of the repeating unit (monomole). To determine the optimum concentration in which self-aggregation of the sensing probe in solution is less, the concentration dependent emission spectra (1×10^{-3} M to 1×10^{-5} M) was recorded in $CHCl_3$. All the π-conjugated polymers displayed less aggregation behavior with concentration 10^{-5} M as evidenced from concentration-dependent fluorescence study.

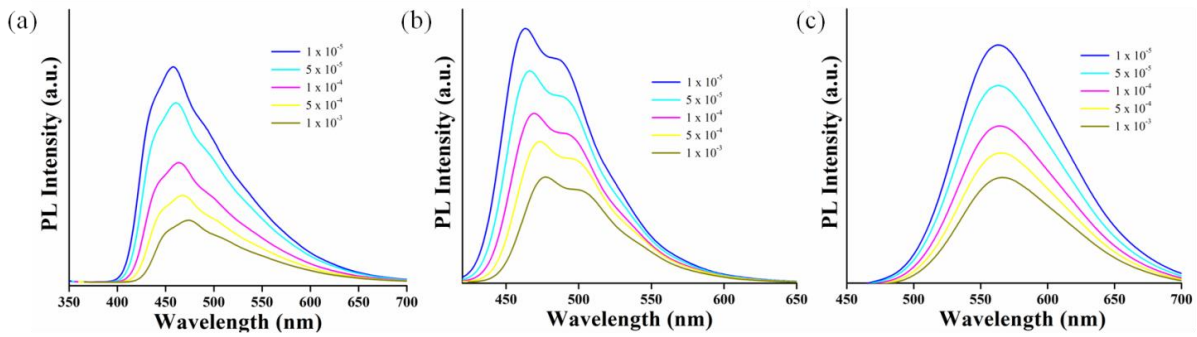

Figure S19: Concentration dependent fluorescence spectra of (a) **P1 (b) P2** and (c) **P3** in $CHCl_3$ at 28 °C.

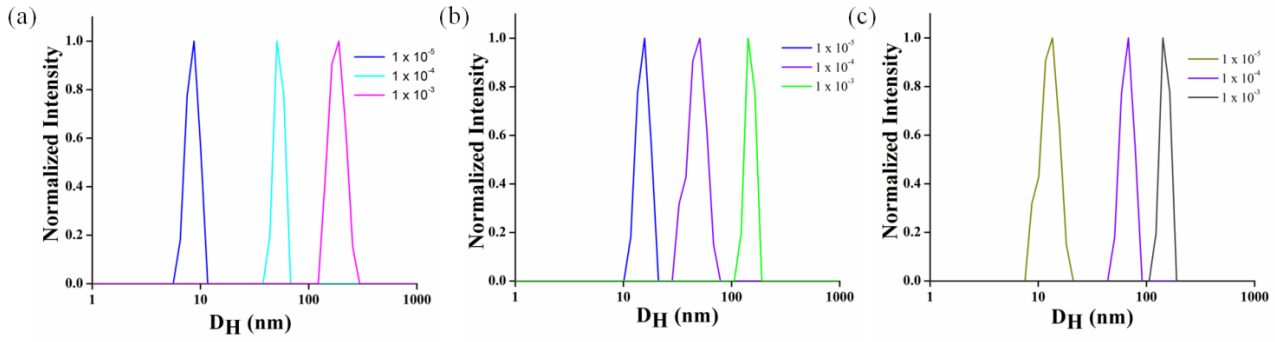

Figure S20: Concentration dependent DLS spectra of (a) **P1 (b) P2** and (c) **P3** in $CHCl_3$ solution at 28 °C. It should be noted that, D_H is derived from a hard sphere model, thus the values obtained for the rigid π-conjugated polymers may not be absolutely correct. However, it is reliable enough for relative comparison between unimers and aggregates.[4]

3d. Fluorescence titration studies of the sensing probes towards NACs

The fluorescence spectroscopic titrations were performed with a continuous variation of concentrations (~1 × 10^{-5} M to ~1 × 10^{-3} M) of NACs in $CHCl_3$ with respect to monomole concentration of the polymer probes.

The percentage of emission quenching of the polymer probes **P1**–**P3** towards different nitroaromatics compounds have been calculated by considering the intensity value of PL spectrum profile of polymer probes towards different nitroaromatics. The details of the calculation are as follows: At first, the value of the emission intensity of the free polymer and polymer-analyte have been estimated at λ_{em} position from the emission quenching experiments Then, the percentage of quenching has been calculated as:

[{(PL Intensity of probe – PL intensity of probe-analyte)/PL intensity of probe} × 100] %.

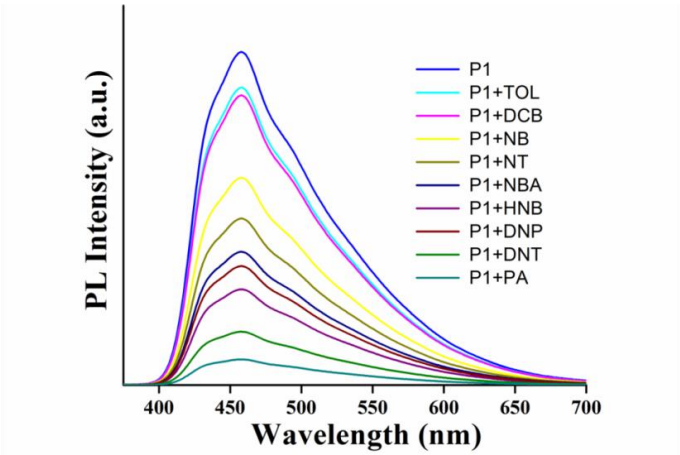

Figure S21: Emission quenching of the polymer **P1** towards different nitroaromatics and non nitroaromatics in $CHCl_3$ solution. Analyte concentration: ~10^{-5} M, polymer: ~1 x 10^{-5} M in $CHCl_3$.

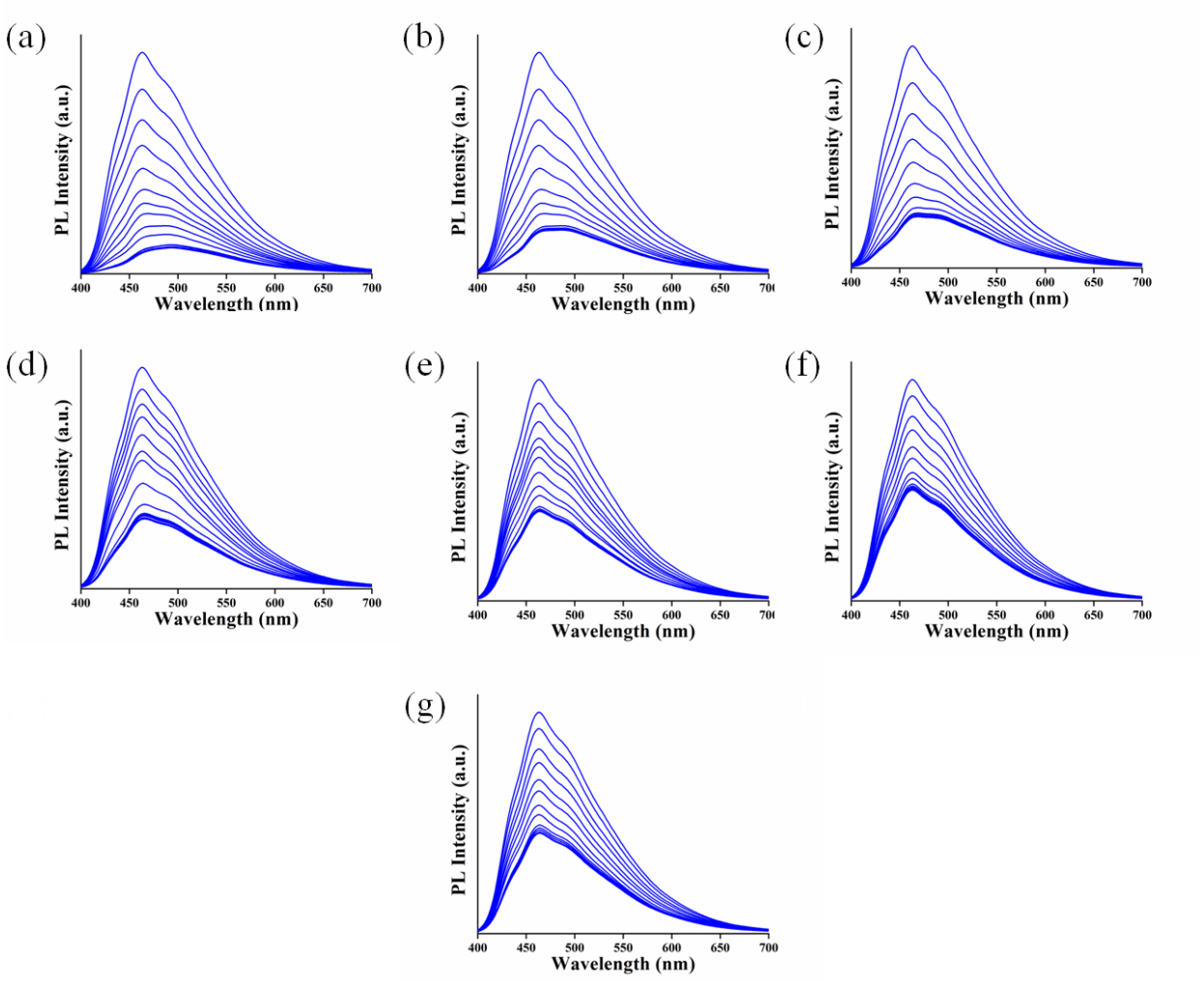

Figure S22: Fluorescence quenching behavior of **P1 (**(~1 x 10^{-5} M in $CHCl_3$) upon incremental addition of (a) picric acid, (b) 2,6-dinitrotoluene, . (c) 2,4-dinitrophenol, (d) 4-nitrobenzoic acid, (e) 4-nitrophenol, (f) nitrotoluene, (g) nitrobenzene with concentration range of NACs: ~1.1 × 10^{-5} M to ~1.2 ×10^{-4} M).

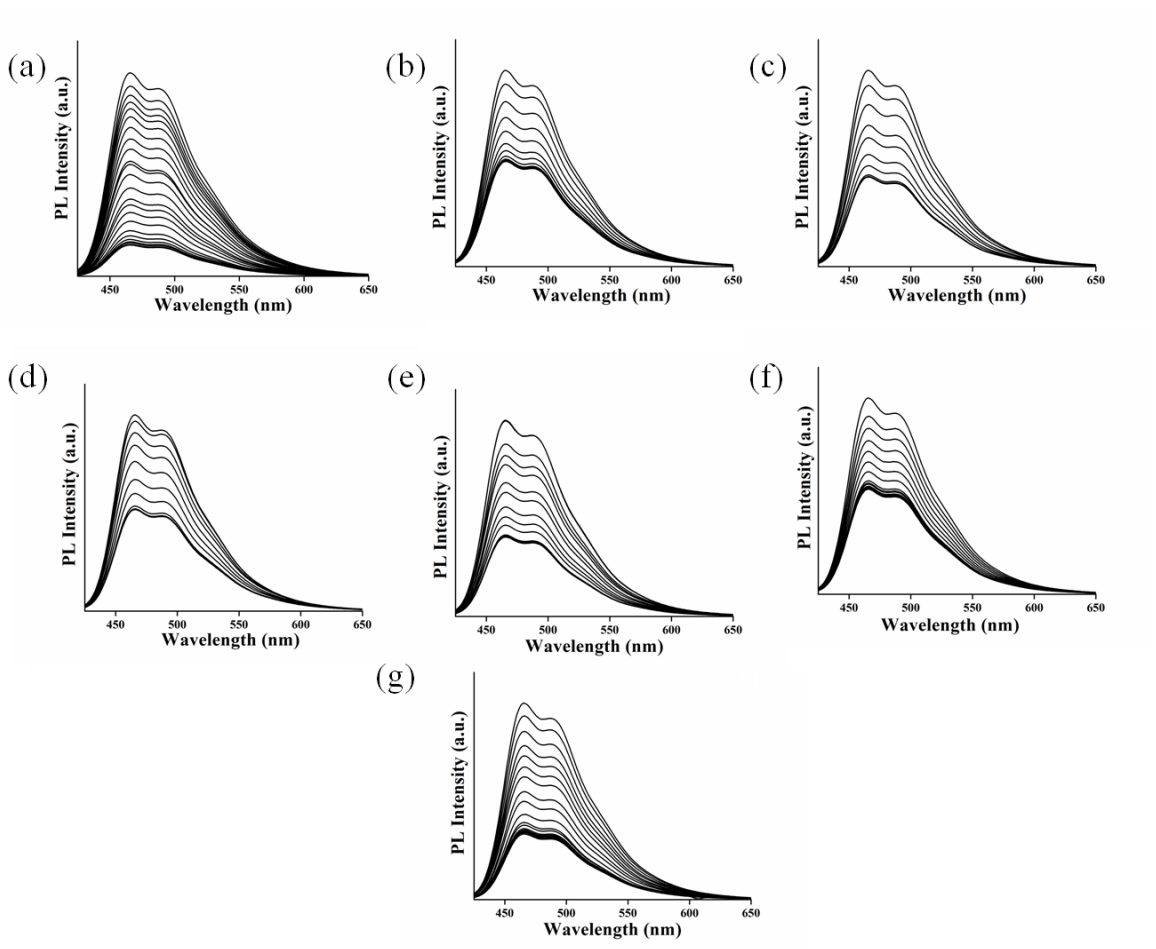

Figure S23: Fluorescence quenching behavior of **P2 ((**~1 x 10^{-5} M in $CHCl_3$) upon incremental addition of (a) picric acid, (b) 2,6-dinitrotoluene, . (c) 2,4-dinitrophenol, (d) 4-nitrobenzoic acid, (e) 4-nitrophenol, (f) nitrotoluene, (g) nitrobenzene with concentration range of NACs: ~1.1 × 10^{-5} M to ~1.2 ×10^{-4} M).

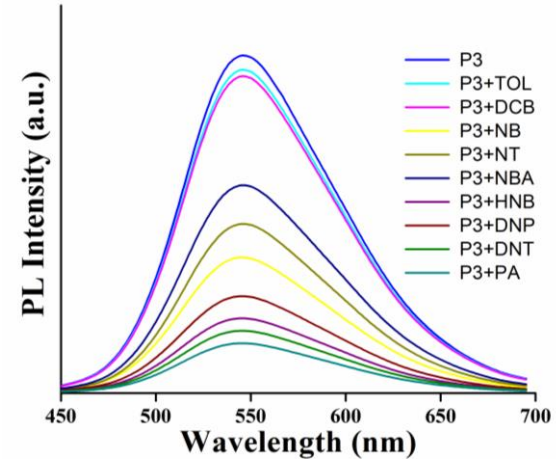

Figure S24: Emission quenching of the polymer **P3** towards different nitroaromatics and non-nitroaromatics in $CHCl_3$ solution. Analyte concentration: ~10^{-5} M, polymer: ~1 x 10^{-5} M in $CHCl_3$.

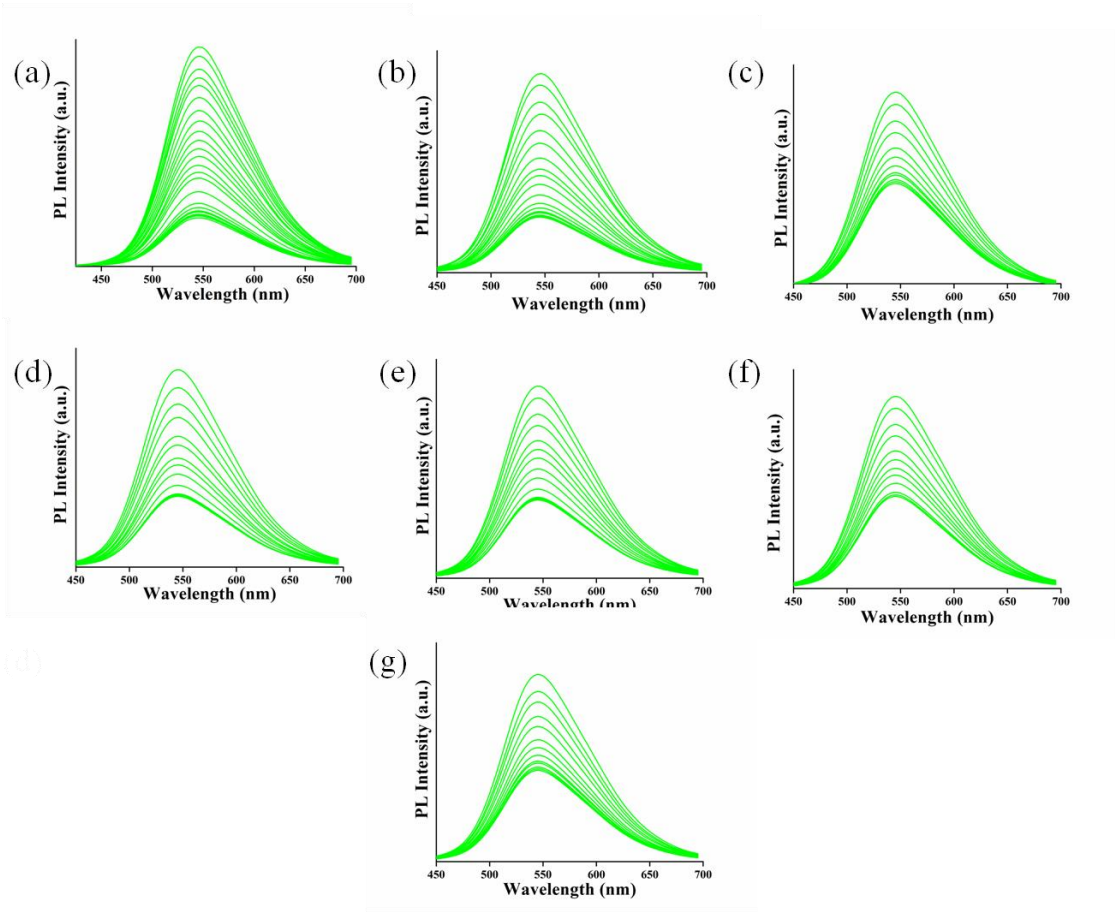

Figure S25: Fluorescence quenching behavior of **P3 ((**~1 x 10^{-5} M in $CHCl_3$) upon incremental addition of (a) picric acid, (b) 2,6-dinitrotoluene, . (c) 2,4-dinitrophenol, (d) 4-nitrobenzoic acid, (e) 4-nitrophenol, (f) nitrotoluene, (g) nitrobenzene with concentration range of NACs: ~1.1 × 10^{-5} M to ~1.2 ×10^{-4} M).

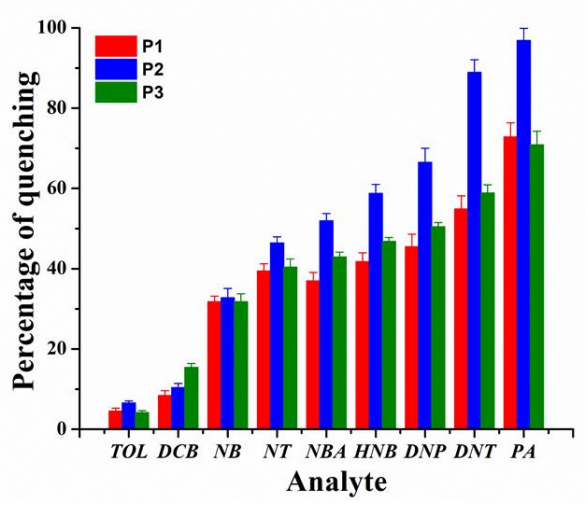

Figure S26: Percentage of emission quenching of **P1**–**P3** towards different nitroaromatics and non-nitro aromatic compounds in $CHCl_3$.Toluene: TOL, 1,2-dichlorobenzene: DCB, Nitrobenzene: NB, Nitrotoluene: NT, Nitrobenzoic acid: NBA, p-Hydroxy nitrobenzene: HNB, 2,4-Dinitrophenol: DNP, 2.6-Dinitrobenzene:DNT, Picric acid: PA.

3e. Calculation of Stern-Volmer constants

The sensitivity of the sensing probes (**P1**, **P2**, **P3)** towards the nitroaromatics was estimated from their Stern-Volmer constants, K_{sv} as determined from the equation:

$$I_o/I = 1 + K_{sv}[Q]$$

I_o and I are the fluorescence intensities in the absence and presence of nitroaromatics respectively, and the Stern-Volmer plots were plotted as a function of the nitroaromatic concentration, [Q]. The Stern-Volmer constants, K_{sv} can be calculated from the slope of the Stern-Volmer plots.

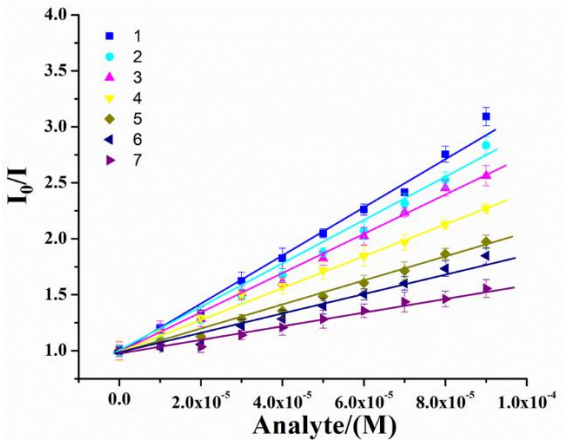

Figure S27: The Stern-Volmer plot for the **P1** towards the different nitroaromatics. 1: NB, 2: NT, NBA, 4: HNB, 5: DNP, 6: DNT, 7: PA.

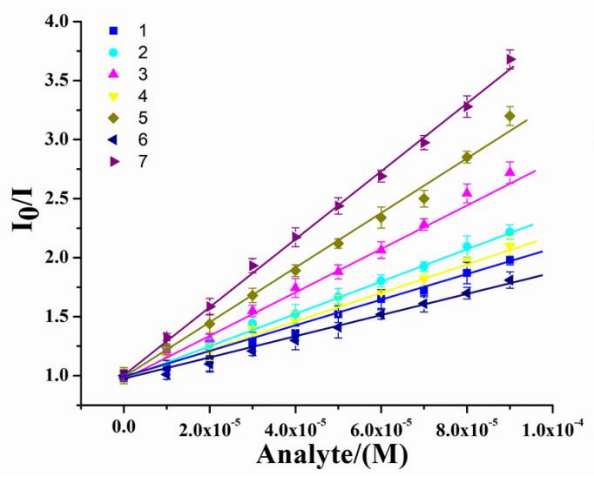

Figure S28: The Stern-Volmer plot for the **P3** towards the different nitroaromatics. 1: NB, 2: NT, NBA, 4: HNB, 5: DNP, 6: DNT, 7: PA.

Table S2: Association constant of **P1, P2** and **P3** towards different nitroaromatics.

Nitroaromatics	**P1 (M^{-1})**	**P2 (M^{-1})**	**P3 (M^{-1})**
Nitrobenzene (NB)	2.58×10^3	4.40×10^3	3.10×10^3
Nitrotoluene (NT)	2.21×10^3	2.11×10^3	2.03×10^3
Nitrobenzoic acid (NBA)	1.16×10^4	1.23×10^4	1.15×10^4
p-Hydroxy nitrobenzene (HNB)	1.45×10^4	1.42×10^4	1.33×10^4
2,4-Dinitrophenol (DNP)	1.71×10^4	2.45×10^4	2.01×10^4
2,6-Dinitrotoluene(DNT)	1.91×10^4	2.66×10^4	2.21×10^4
Picric acid (PA)	2.84×10^4	6.40×10^4	3.10×10^4

3f. Calculation of the limit of detection (LOD)

The limit of detection (LOD) of the sensing probes **(P1, P2** and **P3)** towards nitroaromatics has been determined from emission spectra using the following equation:

$$LOD = 3\sigma/S$$

Here, σ is standard deviation for the blank measurement, and S is the slope of the calibration curve (fluorescence intensity *vs* NAC concentration). The value of σ has been estimated from emission spectra of the free polymer sample without nitroaromatic analytes for an appropriate numbers (8 to 10 times). The get the slope (S), change in fluorescence intensity data at λ_{em} of 458 nm, 464 nm and 551 nm (for **P1**, **P2** and **P3** respectively) was plotted against the concentration of NACs. Emission spectra was recorded by treating NAC solution with varying concentration (*ca.* 10^{-5} M to 10^{-6} M in $CHCl_3$) to the polymer probe of *ca.* 1 x 10^{-5} M in $CHCl_3$. There was a good linear relationship between fluorescent intensity data and concentrations of NACs at micromolar concentration, indicating quantitative detection.

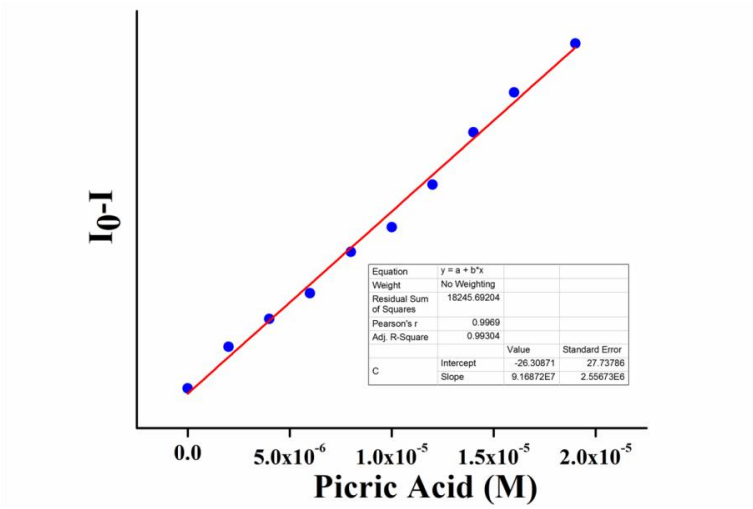

Figure S29: Plot for evaluation of LOD for **P1** towards PA. Change in intensity at λ_{em} of 458 nm with varying concentration of PA was plotted.

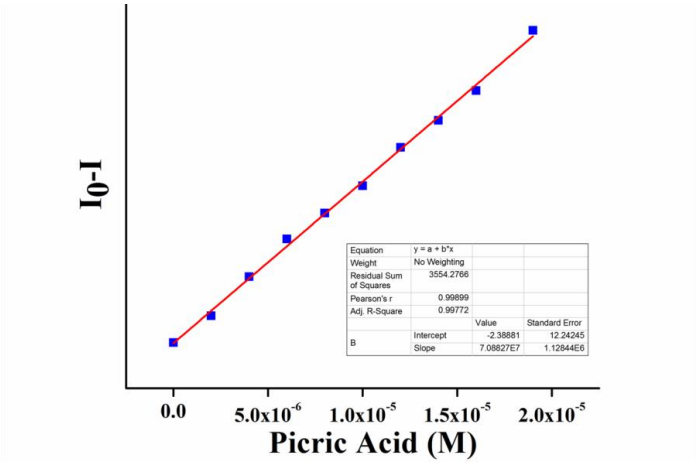

Figure S30: Plot for evaluation of LOD for **P3** towards PA. Change in intensity at λ_{em} of 551 nm with varying concentration of PA was plotted.

Table S3: Limit of detection of **P1, P2** and **P3** towards picric acid.

	P1	**P2**	**P3**
LOD (in M)	9.51×10^{-7}	5.25×10^{-7}	6.21×10^{-7}

3g. Preparation of thin film of the polymer probes for the sensing studies

The quartz substrates ($17 \times 15 \times 1$ mm^3) were cleaned in a fresh piranha solution (7:3 mixture of 98% H_2SO_4 / 30% H_2O_2) followed by ultra-sonication in alkaline isopropanol, 0.1 N aqueous HCl and Milli-Q water for 1 h each. A solution of polymers in chlorobenzene (~3×10^{-4} M) was spin casted on quartz plate at 1000 rpm for 60 second. PL data of the polymer film was measured. After that the film was dipped in different concentration of aqueous picric acid

solution for 10 min followed by repetitive and extensive washing (at least 20 times) by Milli-Q water to remove any unbound (free) picric acid. After drying in air, PL response was recorded.

For the vapor phase study, the thin film of the polymers was exposed to the vapor of the picric acid at room temperature for different time. The PL spectra were recorded with different time interval, after exposing the polymer thin film to the vapor of picric acid in glass chamber. For the film repeatability measurement the polymer film was exposed to the vapor of picric acid for 300 sec and the emission spectrum was recorded. After each measurement, the film was washed with ethanol:water mixture to remove the picric acid and dried under hot air. The emission spectra were recorded and the whole process was repeated for the reputability test.

Figure S31: Experimental setup for demonstrating sensing vapor phase detection of PA at ambient condition.

3h. Detection of aqueous PA sample by polymer thin film probes:

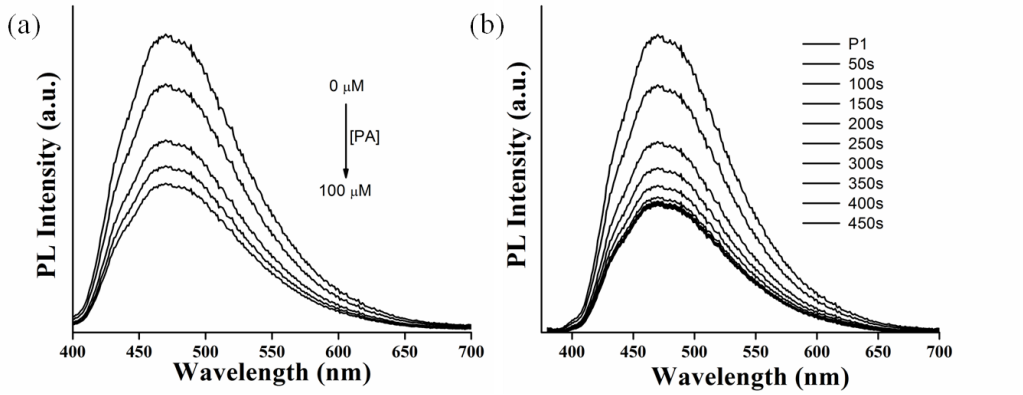

Figure S32: (a) Emission spectra of **P1** (as thin film) after exposing to aqueous PA solution by varying the concentrations. (b) Emission spectra of **P1** (as thin film) after exposing with PA vapour for different time.

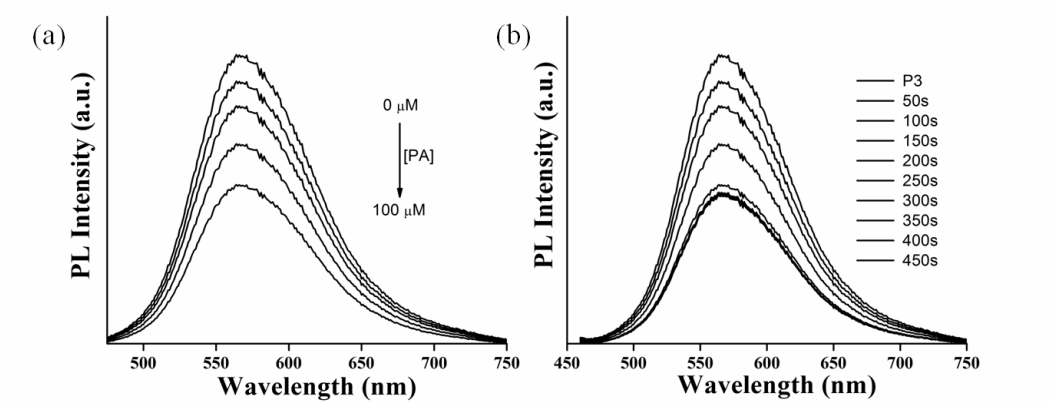

Figure S33: (a) Emission spectra of **P3** (as thin film) after exposing to aqueous PA solution by varying the concentrations. (b) Emission spectra of **P3** (as thin film) after exposing with PA vapour for different time.

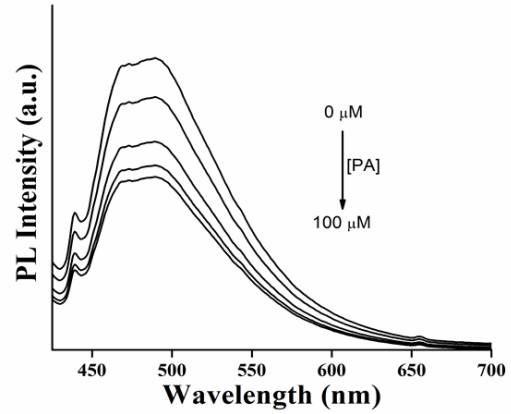

Figure S34: Emission spectra of **P2** (as thin film) after exposing to aqueous PA solution by varying the concentrations.

3i. Repeatability studies

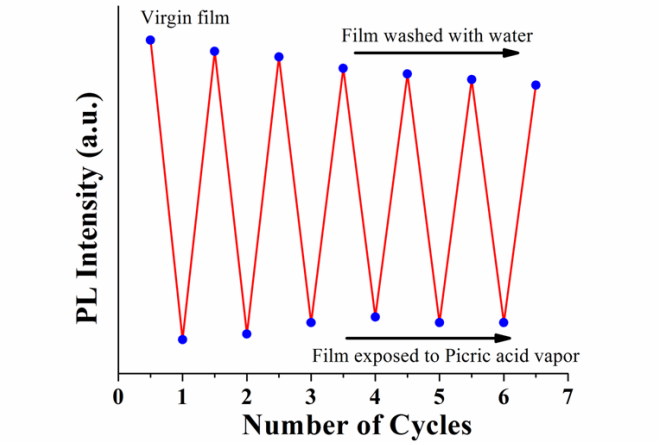

Figure S35: The quenching efficiency of **P1** as a function of reproducibility of sensing ability of polymer thin film to the saturated vapor of PA.

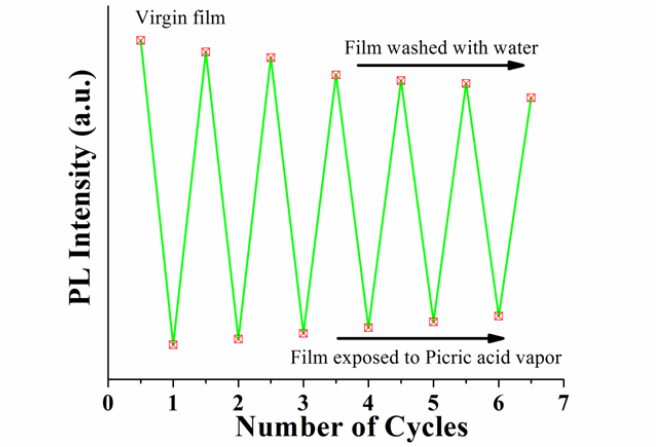

Figure S36: The quenching efficiency of **P3** as a function of reproducibility of sensing ability of polymer thin film to the saturated vapor of PA.

3j. Contact mode detection

For contact mode sensing, Whatman 42 filter paper was cut into small pieces and dipped into concentrated DCM solution of the sensing probes and subsequently dried in air. PA solution of different concentration (10^{-3} – 10^{-9} M) were prepared and 10 µL of each solution was drop-casted on each fresh filter paper strip. When the strips were illuminated under UV at 365 nm, dark spots were observed for PA. The spots were prominent for concentrated samples and slowly faded upon dilution which can be detected by naked eye (under UV illumination at 365 nm). The size of each test strip is 1 cm^2.

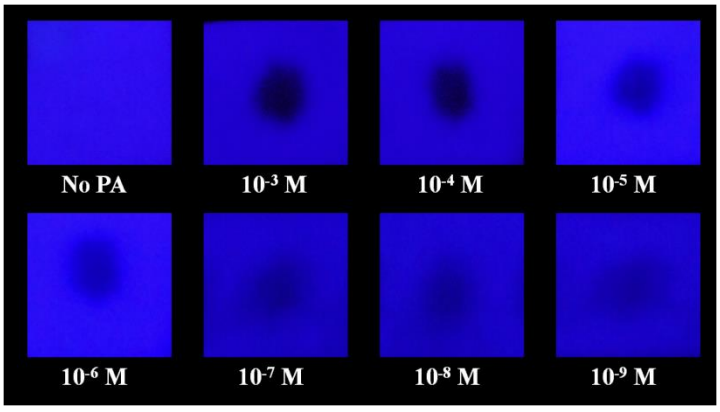

Figure S37: Visual appearance of **P1** coated on filter paper before and after the drop casting of different concentrations of PA by contact mode method under illumination at 365nm light.

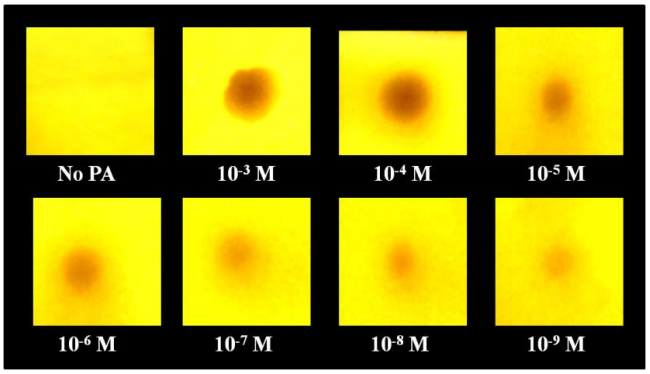

Figure S38: Visual appearance of **P3** coated on filter paper before and after the drop casting of different concentrations of PA by contact mode method under illumination at 365nm.

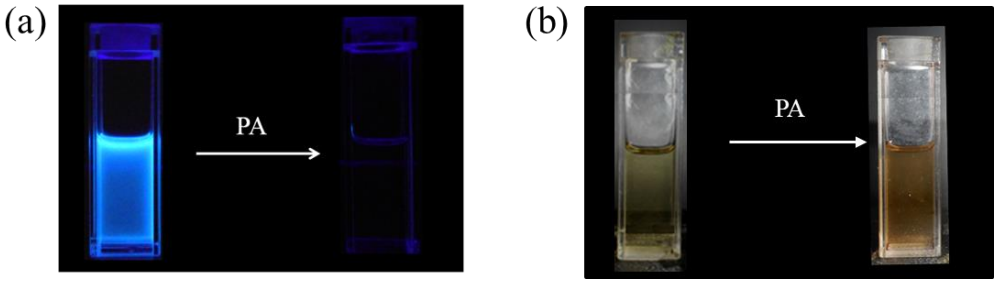

Figure S39: Visual appearance of **P1** before and after the addition of PA under (a) illumination at 365 nm light. (b) under ambient light.

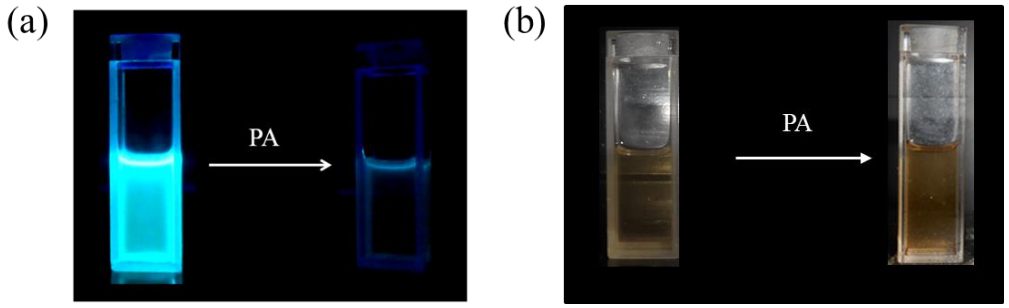

Figure S40: Visual appearance of **P2** before and after the addition of PA under (a) illumination at 365 nm light. (b) under ambient light.

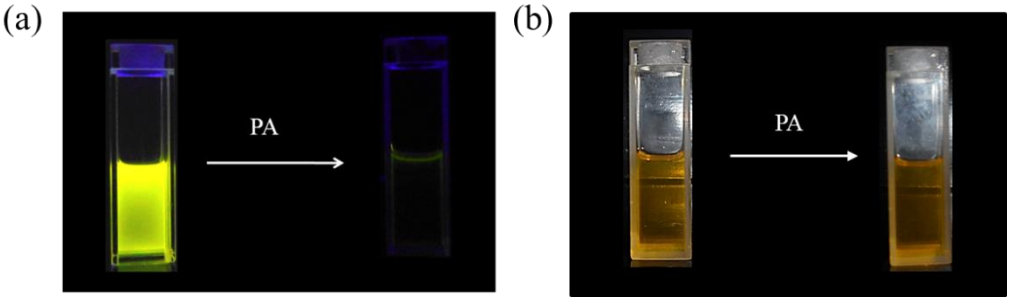

Figure S41: Visual appearance of **P3** before and after the addition of PA under (a) illumination at 365 nm. (b) under ambient light.

4. ^{1}H NMR titration response of the probes towards PA

To investigate the mode of supramolecular interaction between the monomer and NACs, ^{1}H NMR spectroscopic titration studies were carried out with incremental addition of picric acid (PA).

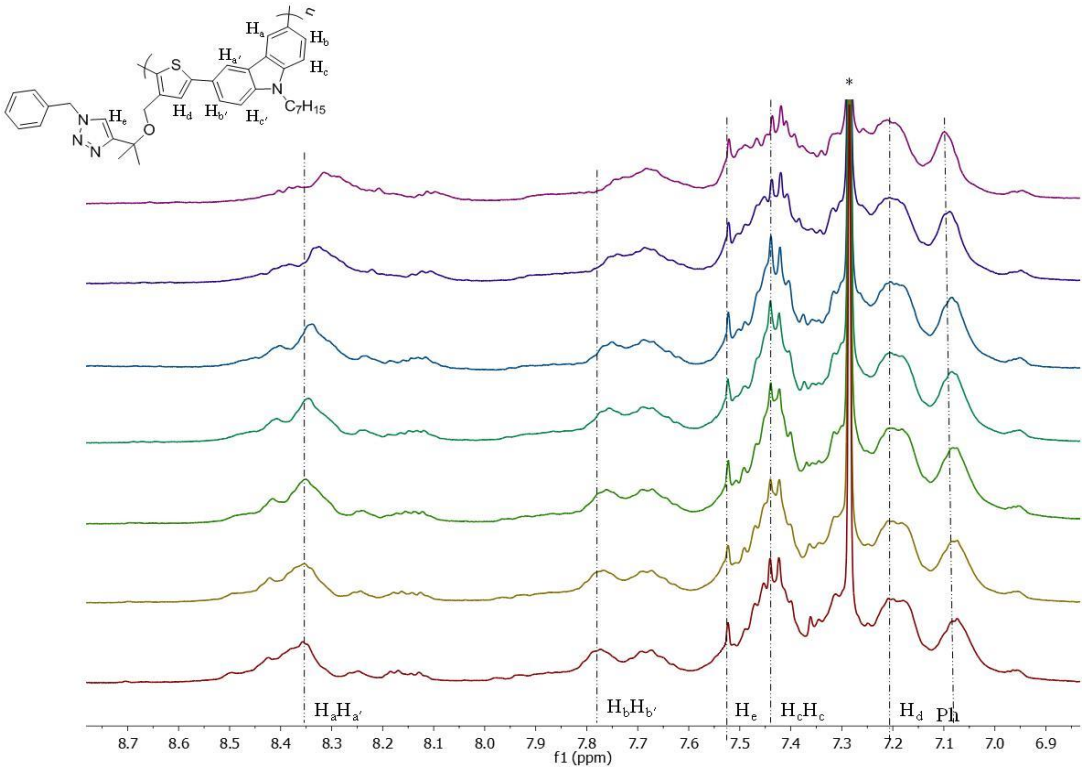

Figure S42: Change in chemical shift of the protons in **P1** during ^{1}H NMR titration in $CDCl_3$ on incremental addition of PA (* = residual $CHCl_3$).

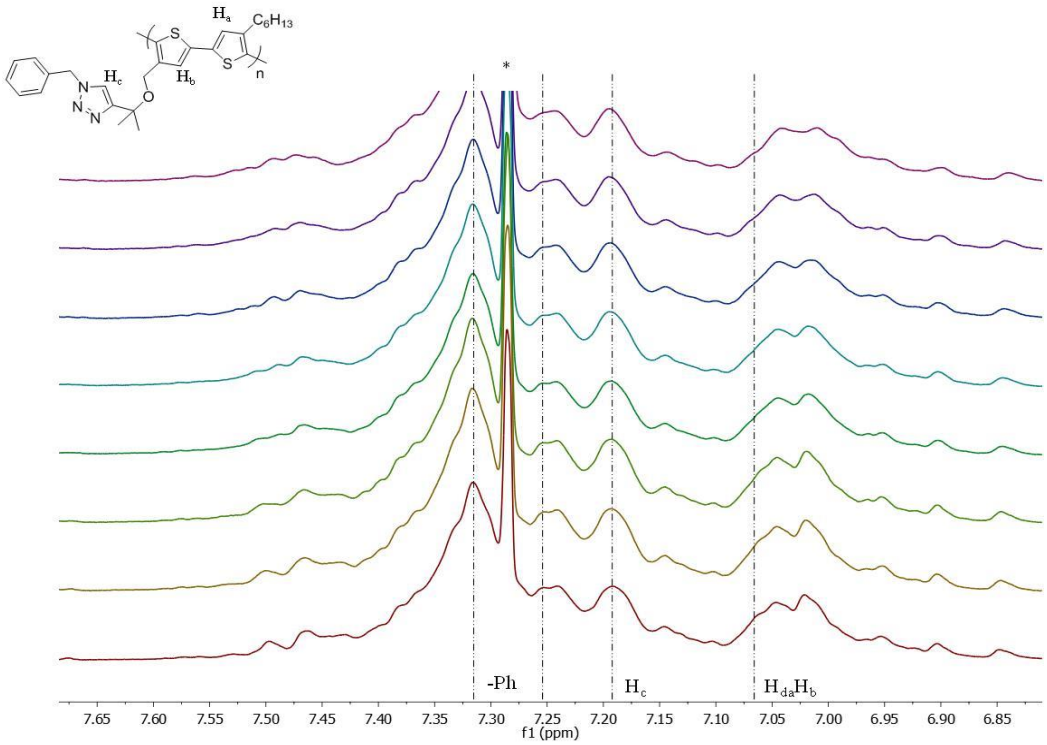

Figure S43. Change in chemical shift of the protons in **P3** during ^{1}H NMR titration in $CDCl_3$ on incremental addition of PA (* = residual $CHCl_3$).

5. Electrochemical characterization

Determination of HOMO and LUMO from CV studies: Cyclic voltammetric analysis was conducted in acetonitrile using Bu_4NPF_6 (0.1 M) as supporting electrolytes, Pt wire counter electrode and Ag/AgCl reference electrode. The solution of **P1, P2** and **P3** were drop casted onto the glossy carbon disc electrode from their DCM solutions. The HOMO energy levels for polymer probes were estimated by conventional electrochemical studies. The HOMO energy level (E_{HOMO}) was calculated from the onset oxidation potential (E_{ox}^{onset}) using the following equation: E_{HOMO} (eV) = [E^{ox}_{onset} - $E^{ox}_{(ferrocene)}$] - 4.80, where the energy level was calibrated against the Ag/AgCl couple. The LUMO energy level (E_{LUMO}) was calculated from the E_{HOMO} energy level and its optical band gap following the equation: E_{LUMO} = (E_{HOMO} + E_g^{opt}) eV, as there is no prominent reduction process for the polymer probes.

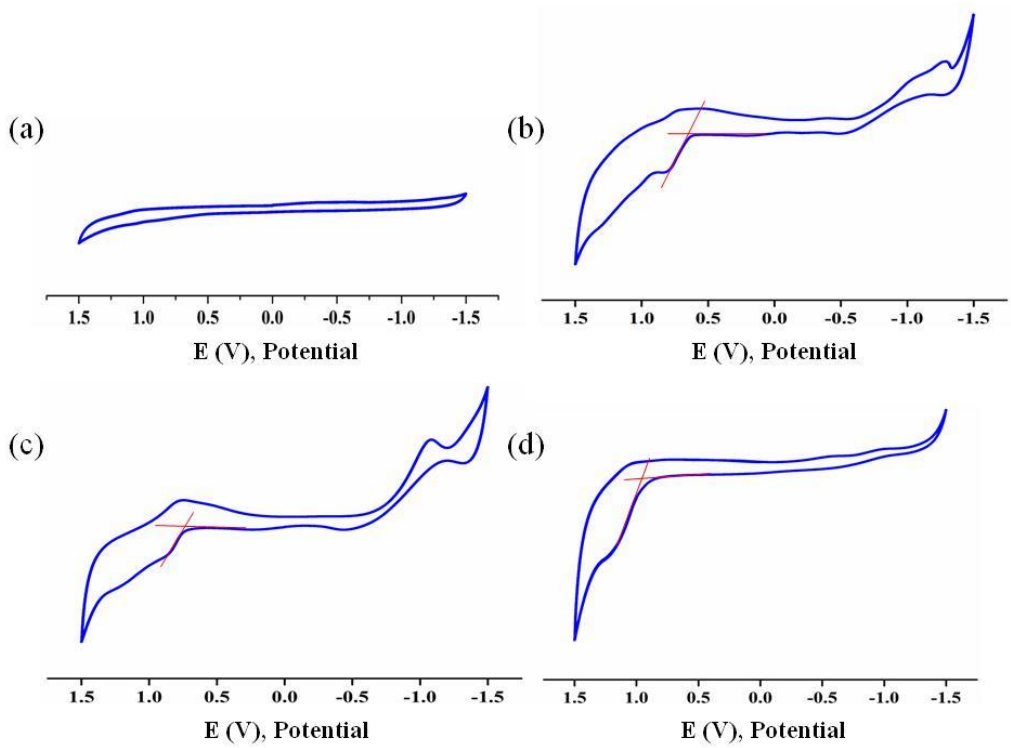

Figure S44: Cyclic voltammogram of (a) acetonitrile (blank run), (b) **P1**polymer film in acetonitrile, (c) **P2** polymer film in acetonitrile and (d) **P3** polymer film in acetonitrile using $TBAPF_6$ as supporting electrolyte, Pt disc working electrode, and Ag/AgCl reference electrode. Scan rate at 100 mV/s.

6. FESEM analysis

Preparation of sample for FESEM analysis: The sample for FESEM analysis was prepared on a clean 1 cm × 1.5 cm aluminium plate. A solution of the probe in chloroform (~5×10^{-4} M) was dropped on the alumina plate and it was dried under a closed chamber for 2 h. The surface morphology was analyzed. The film was dipped in aqueous solution of picric acid derivative (2,4,6-trinitrophenyl 3-bromobenzoate) for 5 min followed by repetitive and extensive washing by Milli-Q water to remove the unbound (free) analyte. After that surface morphology was analyzed.

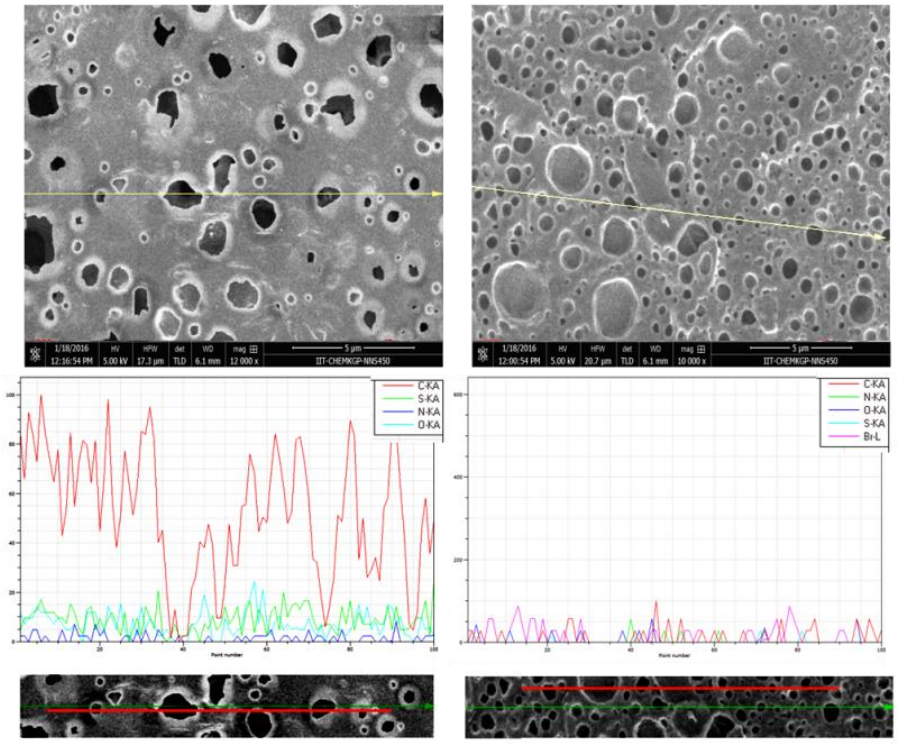

Figure S45: FESEM images of the sensing probes left: **P1**, right: **P1** in presence of picric acid derivative (2,4,6-trinitrophenyl 3-bromobenzoate).

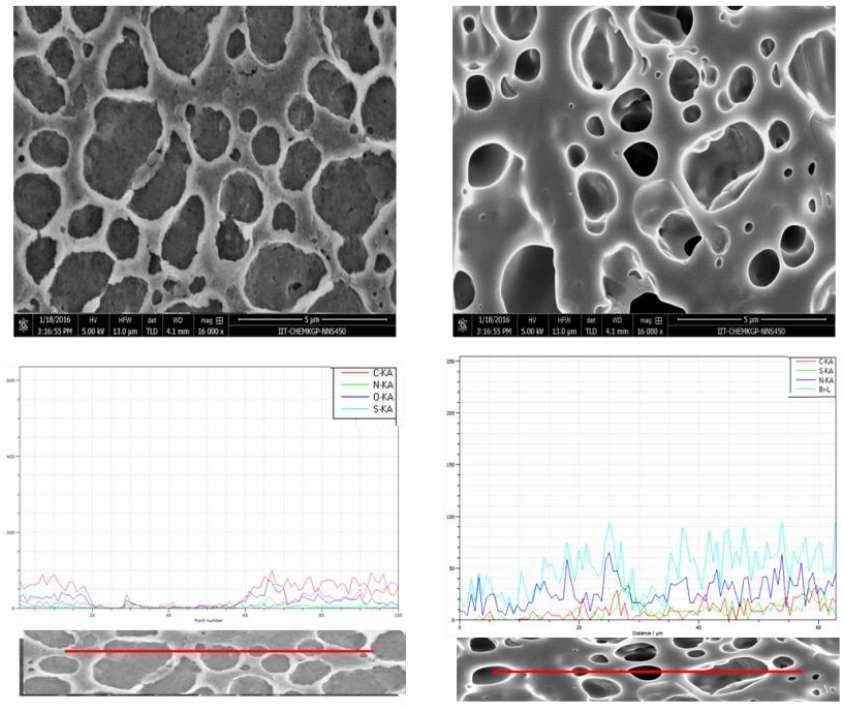

Figure S46: FESEM images of the sensing probes left: **P2**, right: **P2**in presence of picric acid derivative (2,4,6-trinitrophenyl 3-bromobenzoate).

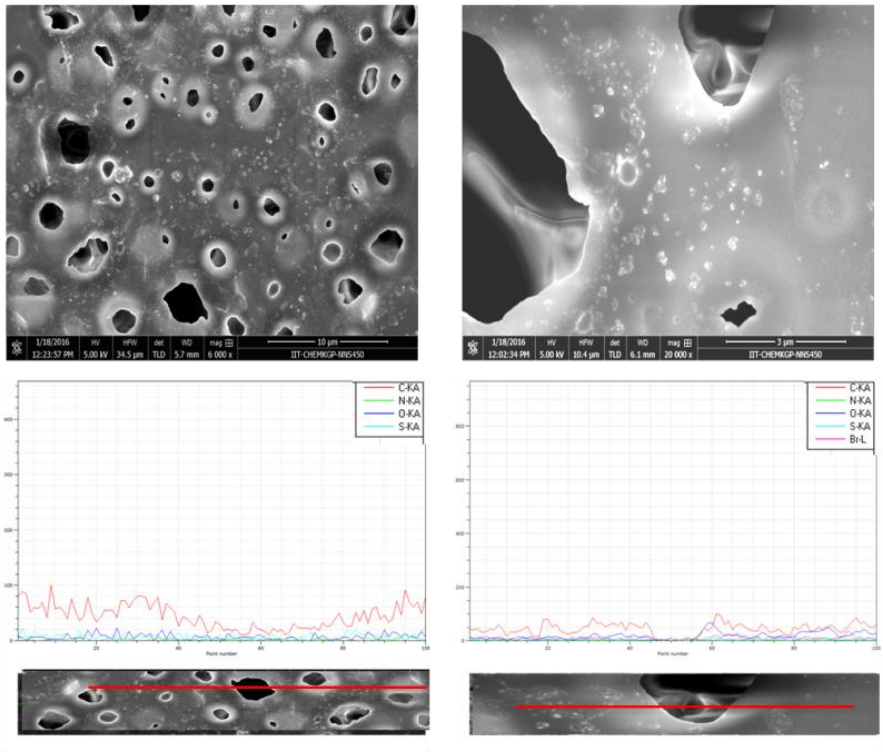

Figure S47: FESEM images of the sensing probes left: **P3**, right: **P3** in presence of picric acid derivative (2,4,6-trinitrophenyl 3-bromobenzoate).

7. Computational studies

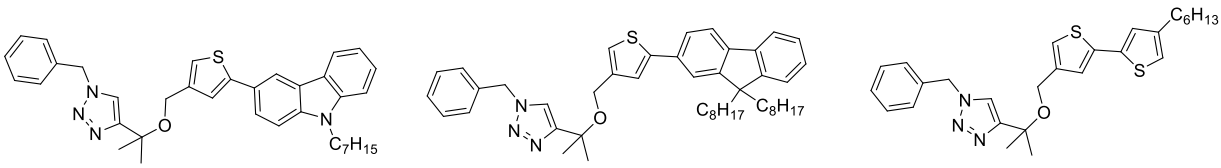

Figure S48: Model probes (**MP1, MP2** and **MP3**) for theoretical studies.

The Density functional theory (DFT) calculation was performed using the Gaussian 09 program based on Becke's three-parameter set with Lee-Yang-Parr correlation functional (B3LYP) and the 6-31G(d,p) basis set for all the model complexes (**MP1, MP2, MP3**). The energy levels of the HOMO/LUMO calculations were executed at the B3LYP structures using the same basis set as those used in the ground-state DFT calculations.[5]

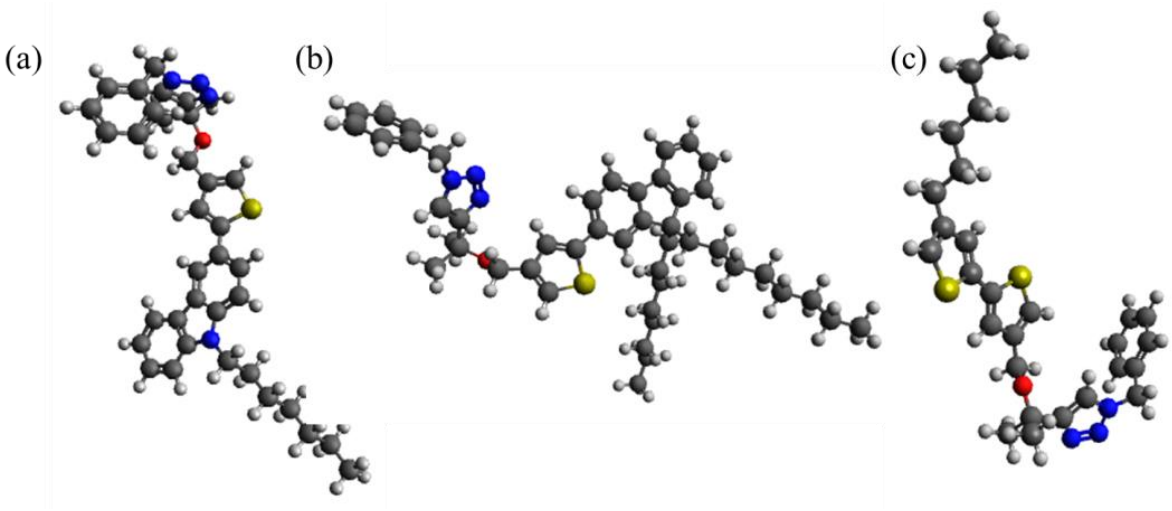

Figure S49: DFT computed optimized structure of model probes (a) **MP1**, (b) **MP2** and (c) **MP3**.

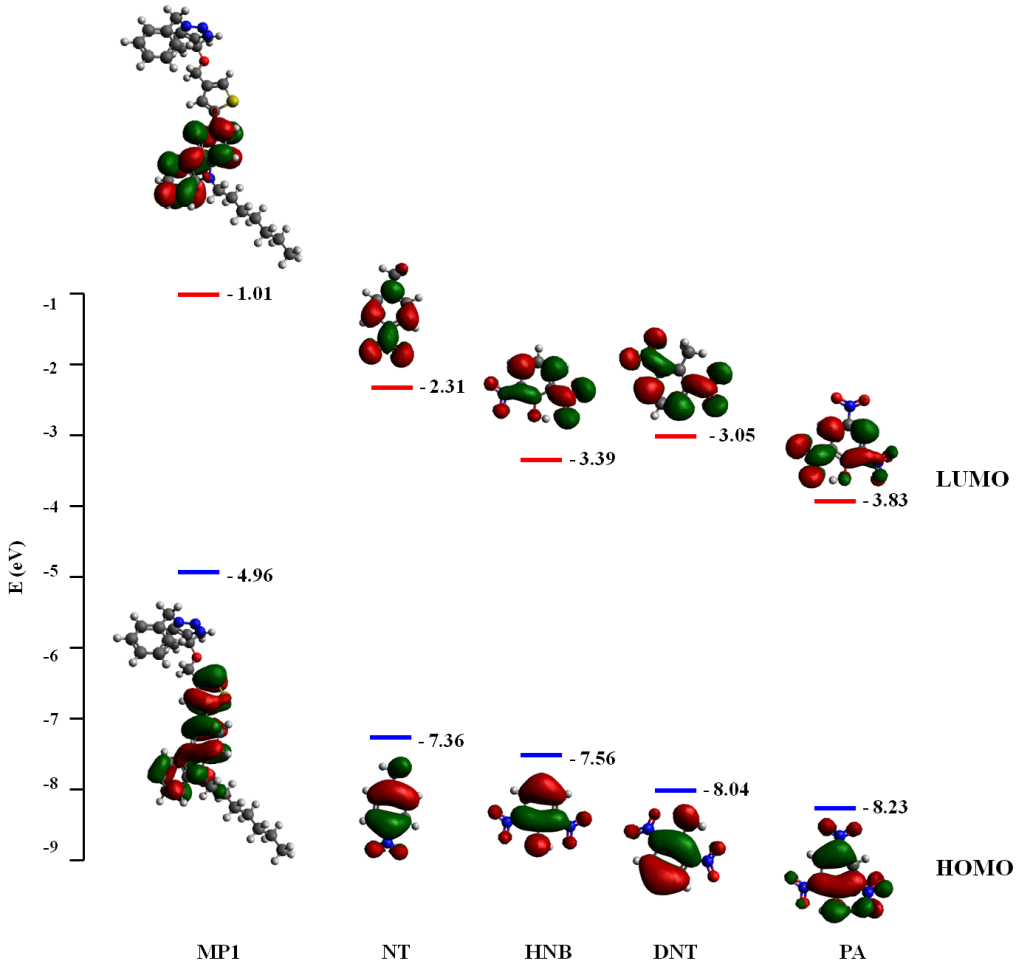

Figure S50a: Calculated HOMO (red) and LUMO (blue) energy level diagram for model complex **MP1** and NACs by DFT, frontier orbital theory using B3LYP functional and polarized 6–31 G⁄basis set.

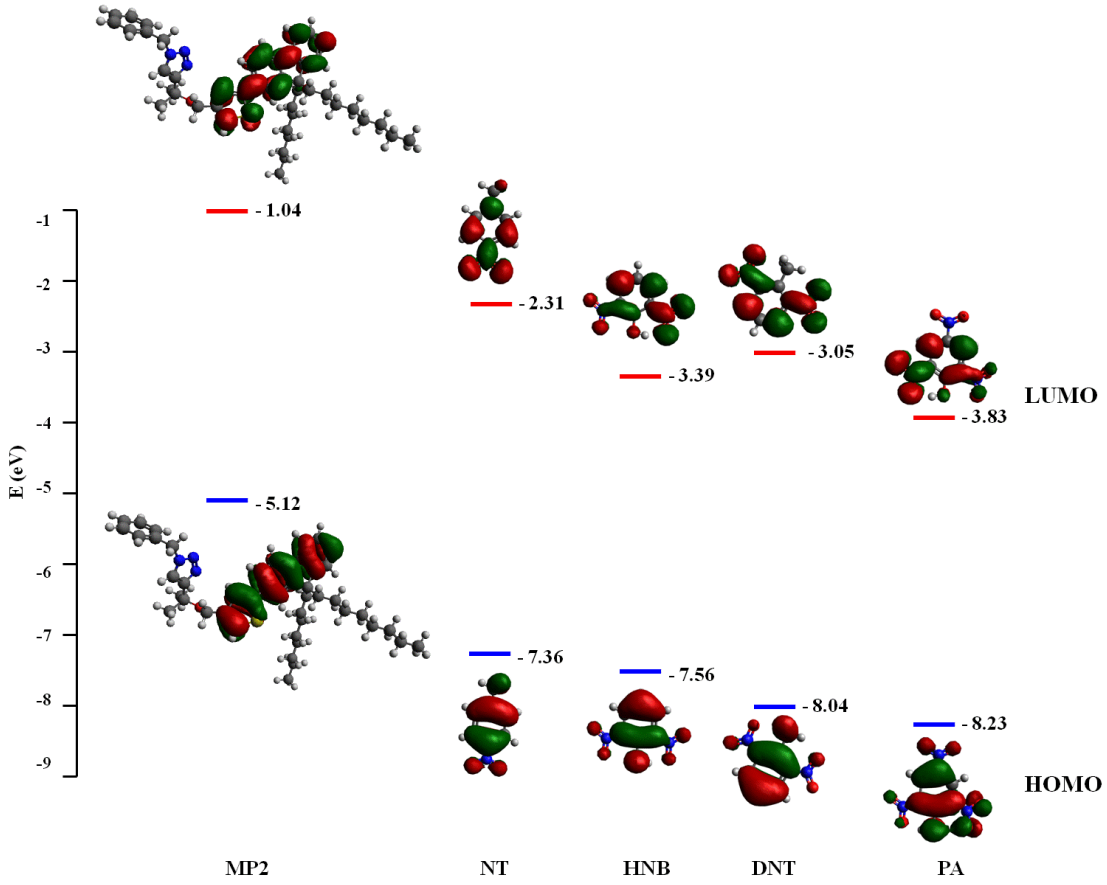

Figure S50b: Calculated HOMO (red) and LUMO (blue) energy level diagram for model complex **MP2** and NACs by DFT, frontier orbital theory using B3LYP functional and polarized 6–31 G⁄basis set.

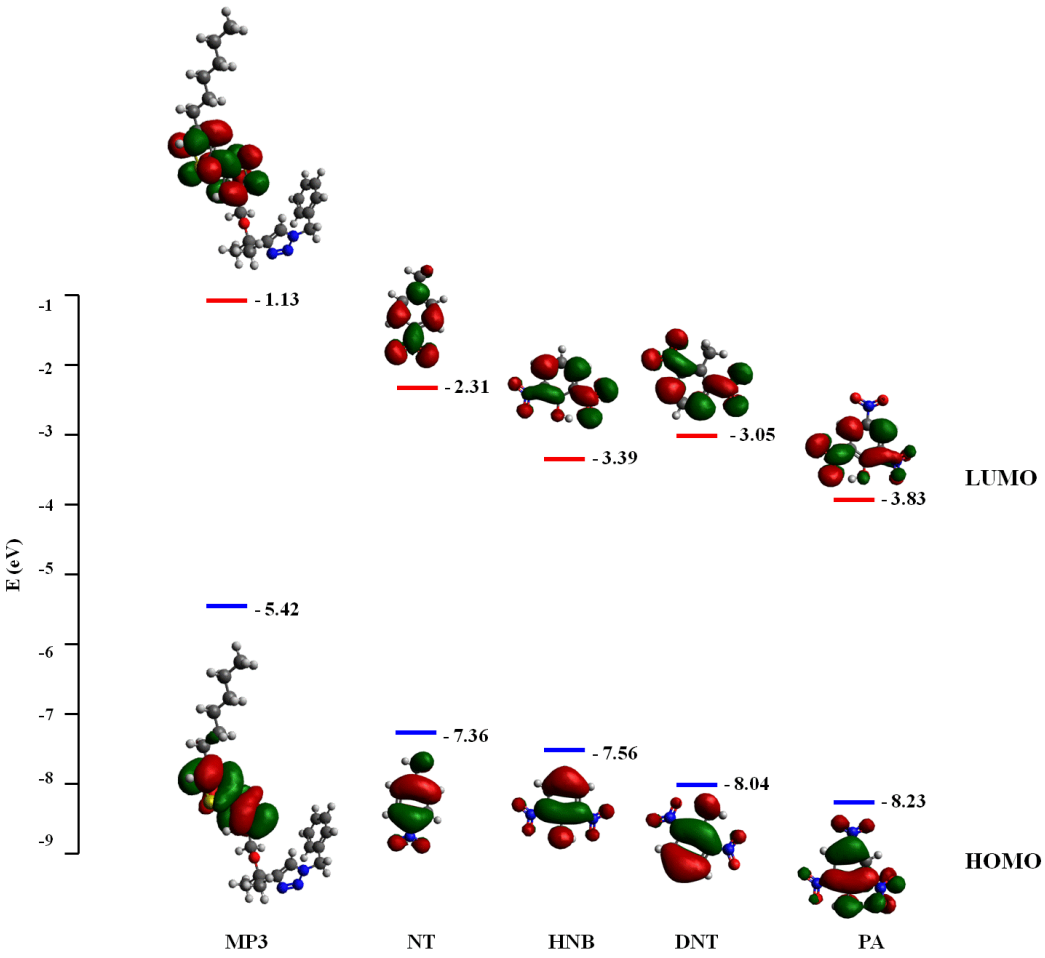

Figure S50c: Calculated HOMO (red) and LUMO (blue) energy level diagram for model complex **MP3** and NACs by DFT, frontier orbital theory using B3LYP functional and polarized 6–31 G⁄basis set.

8. References:

[1] (a) H. Liu, B. Qu, J. Chen, Z. Cong, Z. An, C. Gao, L. Xiao, Z. Chen, Q. Gong, Synthesis of a Terpolymer Containing Fluorene, Side Chain Conjugated Thiophene and Benzothiadiazole and Its Applications in Photovoltaic Devices. J. Appl. Polym. Sci. 128 (2013) 3250. (b) Y. Zou, W. Wu, G. Sang, Y. Yang, Y. Liu, Y. Li, Polythiophene Derivative with Phenothiazine-Vinylene Conjugated Side Chain: Synthesis and Its Application in Field-Effect Transistors. Macromolecules 40 (2007) 7231.

[2] Y. Masuyama, K. Yoshikawa, N. Suzuki, K. Hara, A. Fukuoka. Hydroxyapatite-supported copper(II)-catalyzed azide–alkyne [3+2] cycloaddition with neither reducing agents nor bases in water. Tetrahedron Letters 52 (2011) 6916.

[3] (a) J. R. Lakowicz, Principles of Fluorescence Spectroscopy; Plenum: New York, 1999; Vol. (b) D. F. J. Arago, and J. B. Biot, Mem. Acad. Fr. 1806, 7. (c) A. Chakraborty, D. Chakrabarty, P. Hazra, D. Seth, N. Sarkar, Chem. Phys. Lett. 382 (2003) 508.

[4] (a) S. Holdcroft, *J. Polym. Sci., Part B: Polym. Phys.*, 1991, **29**, 1585. (b) M. Wong, J. Hollinger, L. M. Kozycz, T. M. McCormick, Y. Lu, D. C. Burns and D. S. Seferos, *ACS Macro Lett.*, 2012, **1**, 1266.

[5] (a) Yanai, T.; Tew, D. P.; Handy, N. C. A New Hybrid Exchange-Correlation Functional Using the Coulomb-Attenuating Method (CAM-B3LYP). *Chem. Phys. Lett.***2004**, *393*, 51-57. (b) Frisch, M. J.; Trucks, G. W.; Schlegel, H. B.; Scuseria, G. E.; Robb, M. A.; Cheeseman, J. R.; Scalmani, G.; Barone, V.; Mennucci, B.; Petersson, G. A.; Nakatsuji, H.; Caricato, M.; Li, X.; Hratchian, H. P.; Izmaylov, A. F.; Bloino, J.; Zheng, G.; Sonnenberg, J. L.; Hada, M.; Ehara, M.; Toyota, K.; Fukuda, R.; Hasegawa, J.; Ishida, M.; Nakajima, T.; Honda, Y.; Kitao, O.; Nakai, H.; Vreven, T.; Montgomery Jr., J. A.; Peralta, J. E.; Ogliaro, F.; Bearpark, M.; Heyd, J. J.; Brothers, E.; Kudin, K. N.; Staroverov, V. N.; Kobayashi, R.; Normand, J.; Raghavachari, K.; Rendell, A.; Burant, J. C.; Iyengar, S. S.; Tomasi, J.; Cossi, M.; Rega, N.; Millam, J. M.; Klene, M.; Knox, J. E.; Cross, J. B.; Bakken, V.; Adamo, C.; Jaramillo, J.; Gomperts, R.; Stratmann, R. E.; Yazyev, O.; Austin, A. J.; Cammi, R.; Pomelli, C.; Ochterski, J. W.; Martin, R. L.; Morokuma, K.; Zakrzewski, V. G.; Voth, G. A.; Salvador, P.; Dannenberg, J. J.; Dapprich, S.; Daniels, A. D.; Farkas, Ö.; Foresman, J. B.; Ortiz, J. V.; Cioslowski, J.; Fox, D. J. Gaussian 09, Gaussian Inc., Wallingford, CT, 2009. (c) Reiher, M.; Salomon, O.; Hess, B. A. Reparameterization of Hybrid Functionals Based on Energy Differences of States of Different Multiplicity. *Theor. Chem. Acc.***2001**, *107*, 48-55.